NATIONAL ADVISORY COMMITTEE FOR AERONAUTICS

WARTIME REPORT

ORIGINALLY ISSUED
August 1942 as
Advance Restricted Report

THE EFFECT OF PROPELLER OPERATION ON THE AIR FLOW IN THE REGION OF THE TAIL PLANE FOR A TWIN-ENGINE TRACTOR MONOPLANE

By Harold H. Sweberg

Langley Memorial Aeronautical Laboratory
Langley Field, Va.

NACA

WASHINGTON

NATIONAL ADVISORY COMMITTEE FOR AERONAUTICS

ADVANCE RESTRICTED REPORT

THE EFFECT OF PROPELLER OPERATION ON THE AIR FLOW IN THE REGION OF THE TAIL PLANE FOR A TWIN-ENGINE TRACTOR MONOPLANE

By Harold H. Sweberg

SUMMARY

Extensive air-flow surveys have been made in the region of the tail plane of a typical twin-engine tractor monoplane model with tail surfaces removed. The work was done in the NACA full-scale wind tunnel. The surveys were made with propellers removed and operating and for both cases included the conditions for flaps retracted and flaps deflected 50°. A discussion of the slipstream distortion and the general slipstream effects is given, together with tables and charts of the average downwash angles and the average dynamic pressures at the hinge line of the horizontal tail surface.

Within the boundaries of the slipstream, the average dynamic pressure measured across the horizontal-tail span changed rapidly with the vertical location of the tail plane, but the average downwash angle did not vary greatly with this location. With flaps retracted, the downwash behind the upgoing propeller blades was decreased; whereas the downwash behind the downgoing propeller blades was increased. At normal locations of the horizontal tail surface, the change of downwash angle caused by the slipstream rotation was reversed when the flaps were deflected.

INTRODUCTION

The effects of the propeller slipstream on the stability characteristics of an airplane are conveniently considered in three parts:

(1) The change in lift and pitching moment at the wing

(2) The increase in dynamic pressure at the tail

(3) The change in downwash angle at the tail

For the change in wing lift, the semiempirical methods of reference 1 appear to give results in fairly good agreement with experimental data. With flaps retracted, the change of pitching moment due to the passage of the slipstream over the wing is usually small and may be neglected. With flaps deflected, the change of pitching moment at the wing is considerable and may be estimated from a knowledge of the airfoil section characteristics and the increased velocity over the part of the wing immersed in the slipstream. No generally satisfactory methods exist, however, for predicting the change in air flow at the tail; although the problem has received considerable study (references 2, 3, and 4).

In order to obtain some systematic data relative to the effects of propeller operation on the air flow at the tail, extensive tests of a twin-engine tractor monoplane model have been made in the NACA full-scale wind tunnel. The tests included both force measurements and air-flow surveys, of which only the air-flow surveys are presented in the present paper.

The tests are part of an investigation being conducted by the NACA full-scale wind tunnel to determine the effects of propeller slipstream on the stability characteristics of various types of aircraft. Some investigations of single-engine operation have been reported in references 4 and 5.

SYMBOLS

C_L lift coefficient

$T_c = \frac{\text{effective thrust}}{\rho V_o^2 D^2}$, thrust coefficient

D propeller diameter

ρ density of air

V_o free-stream velocity

D' drag with propellers removed

D_r resultant drag with propellers operating

V local velocity

q_o free-stream dynamic pressure $\left(\frac{1}{2}\rho V_o^2\right)$

q local dynamic pressure $\left(\frac{1}{2}\rho V^2\right)$

q/q_o ratio of local dynamic pressure at tail to free-stream dynamic pressure

$\left(q/q_o\right)_{av}$ average dynamic-pressure ratio across elevator hinge line as found from air-flow surveys

ϵ local downwash angle at tail measured relative to free-stream direction

ϵ_{av} average downwash angle across elevator hinge line as found from air-flow surveys

α_T angle of attack of thrust axis, degrees

S wing area

n propeller rotation speed

d lateral distance between center lines of propeller shafts

b_t span of horizontal tail surface

z distance of elevator hinge line, measured normal to relative wind, from wake center line

h downward displacement, measured normal to free-stream direction, of center line of wake and trailing vortex sheet from its origin at trailing edge of wing

DESCRIPTION OF MODEL AND TESTS

The NACA full-scale wind tunnel is described in reference 6 and the methods by which the data were corrected for jet-boundary and blocking effects are discussed in references 7 and 8.

The model was designed and constructed in the laboratories of the NACA and can be tested as a single-engine, a twin-engine, or a four-engine tractor monoplane. Provision is also made for various positions of the wing and of the horizontal and vertical tail surfaces. For the present series of tests the model was arranged as a twin-engine tractor midwing monoplane having two left-hand three-blade propellers. The thrust line of the propellers is coincident with the wing chord line. A photograph of the model mounted in the wind tunnel is shown in figure 1. Figure 2 is a three-view drawing giving the important dimensions of the model. A summary of additional characteristics of the model follows:

Wing area, square feet	188
Wing profile:	
Root section	NACA 0018
Tip section	NACA 0009
Mean chord, feet	4.95
Aspect ratio	7.69
Taper ratio	2.5:1
Flap deflection, degrees	50
Propeller diameter, feet	5.75
Distance between propeller shafts, feet	11.21
Blade-angle setting at 21-inch (0.61R) radius, degrees	20
Split trailing-edge flaps	
Cuffs mounted on propellers	

Both the vertical and the horizontal tail surfaces were removed for the surveys. The propellers-removed surveys were made with nacelles both on and off, but all the propellers-operating surveys were made with nacelles off.

Power was supplied to the propellers from a 110-horsepower automobile engine in the fuselage by means of an automobile transmission and drive shafts. An electrically operated throttle control made it possible to vary the engine speed from the test house below the model.

The surveys were made with a rack of fifteen 3/8-inch steel survey tubes (fig. 3) spaced 6 inches vertically and 1 foot horizontally. Each tube is constructed in such a way that it measures the total pressure, the static pressure, the angle of pitch, and the angle of yaw of the local air stream. Simultaneous readings of all the tubes were taken by means of a multiple-tube photographic manometer. The survey tubes were calibrated prior to the tests.

The accuracy of the pitch- and yaw-angle measurements is estimated to be approximately $\pm 0.25^{\circ}$; dynamic pressure measurements are accurate to within about ± 1 percent. Check readings were taken frequently during the tests and, in general, were found to be in satisfactory agreement with the original readings. Local fluctuations of the air stream may be the cause of any discrepancies that are shown.

All the surveys were made in the plane of the elevator hinge line. Most of the surveys were made over a large area, but some surveys were limited to measurements across only the elevator hinge line. The surveys were made for propellers-removed and propellers-operating conditions with flaps retracted and with flaps deflected 50°. The range of angles of attack of the model included the complete flight range. For each angle of attack, the thrust of the propellers was varied to include both high and low thrust coefficients; accordingly, the thrust at any particular angle of attack did not necessarily simulate a possible flight condition. Many of the measurements were made at very high thrust coefficients in order to exaggerate the effects of the propeller slipstream.

The thrust coefficient was determined as a function of V/nD for the flaps-retracted condition and is defined as

$$T_c = \frac{\text{effective thrust}}{\rho V_o^2 D^2} = \frac{D' - D_r}{\rho V_o^2 D^2}$$

where both D' and D_r are measured at zero lift coefficient. Figure 4 shows the variation of propeller-thrust coefficient with V/nD.

Some propellers-operating lift curves that cover the range of conditions corresponding to the surveys are shown in figures 5 and 6.

RESULTS AND DISCUSSION

The results of the air-flow surveys are presented in figures 7 to 12. The figures show contours of q/q_o and downwash and sidewash vectors in the plane of the elevator hinge line for various angles of attack. Figures 7 through 10 give the results of the propellers-removed tests. The results, with nacelles off, for flaps retracted and flaps deflected are shown in figures 7 and 8, respectively; the results with nacelles on, for flaps retracted and flaps deflected, are given in figures 9 and 10, respectively. The results of the tests with propellers operating are given in figures 11 and 12. In the following sections, the surveys are discussed with respect to the general nature of the air flow and the slipstream effects. The effects of the slipstream rotation on the downwash angles and the dynamic pressures at the tail are indicated.

Propellers-Removed Surveys

Except for the erratic flow near the rear support just below the fuselage, the propellers-removed surveys (figs. 7 to 10) demonstrate essentially the characteristics of the trailing vortex system discussed in reference 9. Figure 10(c), in particular, shows the complete trailing vortex sheet including the flap-tip and wing-tip vortices and the characteristic deformation of the vortex sheet under the influence of the tip vortices. Other than the deformation, there is relatively little rolling up of the vortex sheet; that is, the flap-tip and wing-tip vortices remain in approximately the same lateral position as at their origins. The wake (or region of low dynamic pressure) coincides with the vortex sheet (across which the lateral component of velocity undergoes an abrupt change). The downwash angles above the wake exceed in magnitude those below the wake.

A comparison of the downward displacement of the wake center from its origin at the trailing edge with the theoretical displacement computed from the charts of reference 10 is given in table I. The measured values are in satisfactory agreement with the theory. The values of the average dynamic-pressure ratio $(q/q_o)_{av}$ across the span of the horizontal tail surface are also included in table I. With increasing angle of attack the wing wake rises relative to the tail (figs. 9(a) to 9(d)) and crosses the tail at

about $\alpha_T = 3.2^\circ$, for which angle the average dynamic-pressure ratio at the tail is, accordingly, a minimum. The center line of the wing wake is always below the tail for the flaps-down condition, progressively approaching the tail as the angle of attack increases. Nacelles tend slightly to reduce the dynamic pressure at the tail.

A comparison of the average downwash angles measured at the elevator hinge line with the theoretical values calculated from the charts of reference 10 is given in table II. The agreement between the measured and the calculated downwash angles is satisfactory (within 1°) for most cases. The presence of engine nacelles caused very little change in the downwash angle measured at the tail plane at low angles of attack. At high angles of attack, however, local stalling of the wing in the region of the nacelles, as observed in tuft surveys, resulted in an appreciable decrease in the downwash angle at the tail.

Propellers-Operating Surveys

The propellers-operating surveys (figs. 11 and 12) show certain characteristic distortions of the slipstream and the air flow in the vicinity of the slipstream. Investigations in Germany reported in references 3 and 11 have identified a number of the factors that produce these effects. Chief among these factors is the splitting, by the wing, of the slipstream into two parts, which, owing to their tangential-velocity components, undergo a lateral displacement from the propeller axis before reuniting at the trailing edge. The nonuniformity of thrust distribution at the propeller disk; the irregular lift distribution across the part of the wing immersed in the slipstream; and the wing, flap, and fuselage wakes may be responsible for some additional elements of distortion of the slipstream.

When the parts of the slipstream that pass above and below the wing are about equal, the result of their lateral displacement at high thrust is the characteristic "figure-eight" slipstream of figures 11(e) to 11(h). For the flaps-deflected condition, owing to the strong upwash in front of the wing, most of the slipstream is carried above the wing, retaining its nearly circular form and undergoing but slight displacement; whereas a small part passes below the wing and is considerably displaced in the direction of its tangential velocity. Somewhat similar patterns have

been observed (reference 4) behind low-wing single-engine monoplanes where the larger part of the slipstream also passes above the wing. The flap-tip vortex also appears to have considerable influence on the lower part of the slipstream. As figures 12(a) to 12(h) show, there is a tendency for this part of the slipstream to flow outward around the flap tip-vortex.

Figures 12(a) to 12(d) show that, as the angle of attack of the model is increased, there is a progressively higher concentration of thrust on the side of the downgoing blade than on the side of the upgoing blade. Because the thrust is not symmetrically distributed within the propeller disk, the slipstream is probably not quite symmetrical even at its origin. The dissymmetry of thrust arises from the inclination of the propeller axis to the air stream, which causes both the local relative airspeed and the local angle of attack to be higher on the side of the downgoing blades than on the side of the upgoing blades. This effect should be greater for the flaps-deflected than for the flaps-retracted condition, because of the greater upwash in front of the wing.

For the flaps-retracted condition, the original direction of rotation of the slipstream is retained to a large extent at the tail. For the flaps-deflected condition, however, the rotation appears in the surveys to have reversed in the region of the tail; that is, the downwash is greatest behind the upgoing blades. This reversal appears not to have been heretofore described.

The slipstream shapes and the velocity distributions obtained in England in 1938 for a very similar model with flaps retracted are in remarkably close agreement with the results presented herein.

Some quantitative evaluations of the dynamic pressures and downwash angles are given in the following sections.

Average dynamic-pressure ratio at tail.- Inasmuch as the average dynamic-pressure ratio $(q/q_0)_{av}$ for a tail plane immersed in the slipstream will vary with the vertical location and the span of the horizontal tail surface, values of the average dynamic-pressure ratio have been computed from the surveys for two horizontal tail surfaces of different span located at three different vertical distances from the fuselage center line. The two spans chosen were (1) the distance between propeller shafts (approximately the

span of the horizontal tail surface used on this model), and (2) the sum of the distance between the propeller shafts and one-half the propeller diameter. The vertical positions chosen were (1) at the hinge line of the actual tail tested, which will be referred to hereinafter as the "reference hinge line"; (2) 6 inches above the reference hingeline; and (3) 12 inches above the reference hinge line. Table III gives the results of the q/q_o measurements averaged across the complete tail spans. Some computations of $(q/q_o)_{av}$ were made across each semispan of the horizontal tail surface in order to determine the effects of direction of propeller rotation. The results showed only small differences in the average dynamic-pressure ratios for the two semispans.

A comparison of the data contained in table III shows that the average dynamic-pressure ratio at the tail plane changed rapidly with the vertical location of the tail plane. The average dynamic-pressure ratio was greatest when measured at the reference hinge line. Measurements taken 6 inches and 12 inches above the reference hinge line showed progressively smaller $(q/q_o)_{av}$ values. For this model, the decrease of $(q/q_o)_{av}$ with increasing height of the tail results from the position of the slipstream, which is mainly below the reference hinge line for all conditions.

Within the boundaries of the slipstream, any increase in the horizontal-tail span will tend to increase the value of $(q/q_o)_{av}$ measured across the tail span. Above or below the slipstream boundaries, however, no change in $(q/q_o)_{av}$ can be obtained by further increases in the horizontal-tail span. The increase of $(q/q_o)_{av}$ with increasing tail span for a tail plane immersed in the slipstream is relatively small (of the order of 10 percent for the two spans considered). Considerations of the effect of increasing the horizontal-tail span on the average downwash angle measured across the tail span, which will be discussed in the next section, may be of somewhat greater importance.

For all cases, the values of $(q/q_o)_{av}$ at the tail plane when the flaps were deflected 50° were much lower than $(q/q_o)_{av}$ when the flaps were retracted. A study of the propellers-operating surveys (figs. 11 and 12) will

show that the slipstreams were displaced farther below the reference hinge line with flaps deflected than with flaps retracted. As a result, the tail plane was located either on the edge of the slipstream or entirely outside the slipstream boundaries when the flaps were deflected.

The surveys indicate that, for constant thrust coefficient, the vertical position of the center line of the slipstream, relative to the reference hinge line, did not remain constant but moved upward toward the reference hinge line with increasing angle of attack. Although this upward displacement of the slipstream center line was relatively small, it was nevertheless sufficient to effect an appreciable increase in $(q/q_0)_{av}$ at the tail.

The surveys show that the slipstream was flattened vertically and elongated horizontally. Inasmuch as the lateral boundaries of the slipstream were extended, an increased proportion of the tail-plane area could lie within the slipstream in a certain region of comparatively small depth. Within this region, the dynamic pressure approaches or may exceed the theoretical mean value of $1 + \frac{8T_c}{\pi}$ for a totally immersed tail plane. This condition is illustrated in figure 13. The plotted points were obtained from the measurements taken at the reference hinge line across the larger of the two horizontal-tail spans. The curves of figure 13, for this lowest tail position, most nearly correspond to the condition of a tail plane totally immersed within the boundaries of a slipstream.

Average downwash at tail.- In order to indicate the effects of slipstream rotation, average downwash angles were separately computed for each semispan of the horizontal tail surfaces. The downwash angles have not been weighted according to the variation of local dynamic pressure across the tail span, inasmuch as a few computations showed this correction to be relatively slight. The computations were made for the same spans and the same vertical positions discussed in the previous section. Figures 14 to 19 show the results of these computations.

When the span of the horizontal tail surface is equal to the distance between the center lines of the propeller shafts, the right semispan, viewed from the rear, is affected by the air flow from a downgoing propeller blade; whereas the left semispan is affected by the air flow from an upgoing propeller blade. Figures 14 to 16 show that,

with flaps retracted, the downwash at the tail on the side of the downgoing blade is increased and that the downwash at the tail on the side of the upgoing blade is decreased. From figure 14, a difference of approximately 7° downwash angle was found at the highest value of thrust coefficient $T_c = 1.300$. As the span of the horizontal tail surface is extended past the center lines of the propeller shafts, this difference is decreased although the average downwash angle across the complete horizontal-tail span remains approximately constant. It will also be noticed (figs. 14 to 16) that, with flaps retracted, this difference is greatest at high angles of attack (high C_L). As the angle of attack of the model is increased, a considerably greater part of the slipstream jet will pass over the wing than at low angles of attack. As a result, less of the slipstream rotation will be taken out and the effects of the rotation will consequently be greater at the high angles of attack than at the low angles of attack. That this effect is not evident for the flaps-deflected condition may be due to the low position of the slipstream with respect to the tail.

A comparison of the average downwash angles across the semispan of the horizontal tail surface with flaps deflected 50° (figs. 17 to 19) shows that the downwash on the side of the downgoing blade is considerably less for this condition than the downwash on the side of the upgoing blade. At the highest value of thrust coefficient, $T_c = 1.300$, a difference in ϵ_{av} of approximately 10° was measured between the two semispans. As for the case with flaps retracted, this difference decreases as the span of the horizontal tail surface is increased, although the average downwash angle across the complete horizontal-tail span remains approximately constant.

The difference between the average downwash angles across the two semispans of the horizontal tail surface was considerably reduced as the vertical distance of the tail plane from the reference hinge line was increased. With flaps retracted, at $T_c = 1.300$, a maximum difference of 7.0° was measured at the reference hinge line in comparison with a maximum difference of 4.2° measured 12 inches above the reference hinge line. With flaps deflected 50° at $T_c = 1.300$ a maximum difference of 9.7° was found at the reference hinge line in comparison with a maximum difference of 4.8° at a height of 12 inches above the reference hinge line. Although the difference between the

average downwash angles across the two semispans of the horizontal tail was reduced, the average downwash angle across the complete tail span was found to change very little for the three vertical locations of the horizontal tail considered.

Values of the average downwash angles across the horizontal-tail span plotted against model lift coefficient are shown in figures 20 and 21 for the flaps-retracted and flaps-deflected conditions, respectively. At constant lift coefficient the variation of downwash angle with thrust coefficient is small for most cases (within 1°) for both the flaps-retracted and flaps-deflected conditions.

The downwash measurements indicate that, with flaps retracted, an improvement in the longitudinal stability of a twin-engine airplane can be obtained by the use of oppositely rotating propellers, the blades of which turn upward in the middle. In order to utilize the favorable slipstream rotation, the span of the horizontal tail surface should be approximately equal to the distance between the two propeller shafts. With flaps deflected, however, the use of oppositely rotating propellers, the blades of which turn upward in the middle, may result in a loss of longitudinal stability.

CONCLUDING REMARKS

From measurements of the air flow in the region of the horizontal tail surface of a twin-engine tractor monoplane with propellers operating, the following results are summarized.

1. The presence of the wing behind the propeller disk caused a severe distortion of the velocity distribution within the propeller slipstream. The slipstream was divided into two parts that were displaced laterally and therefore did not reunite into a single circular jet.

2. The average dynamic pressure across the horizontal-tail span changed rapidly with the vertical location of the tail with respect to the slipstream, but the average downwash angle changed only slightly with vertical location of the horizontal tail surface.

3. For certain cases in which the horizontal tail extended across the center of the slipstream, the average dynamic pressure at the tail was found to exceed the theoretical mean value of the dynamic pressure in the slipstream.

4. The center line of the slipstream rose, relative to the tail, with increasing angle of attack.

5. With flaps retracted, the downwash on the side of the horizontal tail surface affected by the upward stroke of the propeller blades was less than the downwash on the side affected by the downward stroke of the propeller blades.

6. For normal locations of the horizontal tail surface, the distribution of downwash at the tail was reversed when the flaps were deflected; that is, the downwash was greater behind the upgoing blades than behind the downgoing blades.

7. The difference between the average downwash angles measured across the two semispans of the horizontal tail surface with propellers rotating in the same direction was reduced when the semispans were extended past the center lines of the propeller shafts; however, the average downwash angle across the complete horizontal tail span remained approximately constant.

8. An improvement in the longitudinal stability of an airplane with flaps retracted might be obtained by the use of oppositely rotating propellers, the blades of which turn upward in the middle.

Langley Memorial Aeronautical Laboratory,
National Advisory Committee for Aeronautics,
Langley Field, Va.

REFERENCES

1. Smelt, R., and Davies, H.: Estimation of Increase in Lift Due to Slipstream. R. & M. No. 1788, British A.R.C., 1937.

2. Katzoff, S.: Longitudinal Stability and Control with Special Reference to Slipstream Effects. Rep. No. 690, NACA, 1940.

3. Stüper, J.: Effect of Propeller Slipstream on Wing and Tail. T.M. No. 874, NACA, 1938.

4. Goett, Harry J., and Pass, H. R.: Effect of Propeller Operation on the Pitching Moments of Single-Engine Monoplanes. NACA A.C.R., May 1941.

5. Pass, H. R.: Wind-Tunnel Study of the Effects of Propeller Operation and Flap Deflection on the Pitching Moments and Elevator Hinge Moments of a Single-Engine Pursuit-Type Airplane. NACA A.R.R., July 1942.

6. DeFrance, Smith J.: The N.A.C.A. Full-Scale Wind Tunnel. Rep. No. 459, NACA, 1933.

7. Silverstein, Abe, and Katzoff, S.: Experimental Investigation of Wind-Tunnel Interference on the Downwash behind an Airfoil. Rep. No. 609, NACA, 1937.

8. Theodorsen, Theodore, and Silverstein, Abe: Experimental Verification of the Theory of Wind-Tunnel Boundary Interference. Rep. No. 478, NACA, 1934.

9. Silverstein, Abe, Katzoff, S., and Bullivant, W. Kenneth: Downwash and Wake behind Plain and Flapped Wings. Rep. No. 651, NACA, 1939.

10. Silverstein, Abe, and Katzoff, S.: Design Charts for Predicting Downwash Angles and Wake Characteristics behind Plain and Flapped Wings. Rep. No. 648, NACA, 1939.

11. Stiess, W.: Über den Einfluss des Luftschraubendrehsinnes auf die Längsstabilität von zweimotorigen Flugzeugen. Jahrb. 1938 der deutschen Luftfahrtforschung, R. Oldenbourg (Munich), pp. I206-I219.

TABLE I

LOCATION OF WAKE CENTER LINE AND VALUES OF THE AVERAGE DYNAMIC PRESSURE RATIO AT ELEVATOR HINGE LINE WITH PROPELLERS REMOVED

Condition	α_T (deg)	C_L	$(q/q_o)_{av}$	z (in.)	h_{exp} (in.)	h_{theor} (in.) (a)
Nacelles on; flaps retracted	-2.3	-0.155	0.94	-8.2	-2	-2
	3.2	.255	.90	0	3	4
	9.6	.741	.92	6.9	11	12
	16.0	1.171	.97	18.0	14	18
Nacelles on; flaps deflected 50°	-2.7	.358	.91	-35.5	18	14
	2.7	.800	.92	-29.5	25	21
	8.9	1.325	.89	-23.5	33	30
	15.2	1.799	.67	-11.4	36	38
Nacelles off; flaps retracted	-2.3	-0.160	.93	-6.0	-4	-3
	3.2	.255	.91	0	3	4
	9.6	.741	.93	6.0	11	12
	16.0	1.191	.95	16.2	16	19
Nacelles off; flaps deflected 50°	-2.7	.358	.96	-35.5	18	14
	2.7	.800	.95	-28.8	24	21
	8.9	1.315	.91	-23.5	33	30
	15.2	1.765	.76	-11.4	36	37

[a]Values from reference 10.

TABLE II

COMPARISON OF EXPERIMENTAL AND THEORETICAL DOWNWASH ANGLES WITH PROPELLERS REMOVED

Condition	α_T (deg)	C_L	ϵ_{av}	ϵ_{theor} (a)
Nacelles on; flaps retracted	-2.3	-0.155	-2.2	-0.9
	3.2	.255	.7	1.5
	9.6	.741	3.1	4.4
	16.0	1.171	3.6	6.9
Nacelles on; flaps deflected 50°	-2.7	.358	3.0	3.7
	2.7	.800	6.2	6.9
	8.9	1.325	9.0	9.7
	15.2	1.799	10.4	12.4
Nacelles off; flaps retracted	-2.3	-.160	-2.0	-1.0
	3.2	.255	.5	1.5
	9.6	.741	3.1	4.4
	16.0	1.191	5.1	7.0
Nacelles off; flaps deflected 50°	-2.7	.358	3.0	4.5
	2.7	.800	6.2	6.9
	8.9	1.315	9.0	9.6
	15.2	1.765	11.4	11.9

[a]Values from reference 10.

TABLE III

AVERAGE DYNAMIC-PRESSURE RATIO AT TAIL

Flaps retracted				Flaps deflected 50°			
α_T (deg)	T_c	$(q/q_o)_{av}$		α_T (deg)	T_c	$(q/q_o)_{av}$	
		$b_t = d$	$b_t = d + \frac{1}{2}D$			$b_t = d$	$b_t = d + \frac{1}{2}D$
Measured at reference hinge line							
-4.1	0.021	1.09	1.12	-4.7	0.021	0.99	0.99
1.4		1.09	1.13	.8		.96	.96
7.7		1.14	1.18	7.1		.94	.94
14.1		1.18	1.26	13.4		.93	.93
-4.1	.161	1.24	1.33	-4.7	.161	.99	.99
1.4		1.33	1.46	.7		1.03	1.04
7.7		1.41	1.56	6.9		1.09	1.12
11.3		1.61	1.70	10.5		1.09	1.13
-4.1	.619	1.85	2.08	-4.8	.619	1.02	1.02
1.3		2.19	2.40	.6		1.16	1.16
7.7		2.39	2.60	6.9		1.45	1.44
14.0		2.86	3.02	13.3		1.44	1.53
-3.9	1.300	2.36	2.61	-5.0	1.300	1.03	1.02
1.4		2.82	3.03	.3		1.31	1.27
7.5		4.23	4.49	6.8		1.51	1.63
11.0		3.45	3.80	9.6		1.51	1.77
Measured 6 in. above reference hinge line							
-4.1	0.021	1.03	1.05	-4.7	0.021	0.98	0.98
1.4		1.13	1.16	.8		.98	.99
7.7		1.09	1.13	7.1		.96	.96
14.1		1.15	1.20	13.4		.95	.94
-4.1	.161	1.14	1.22	-4.7	.161	1.00	1.00
1.4		1.29	1.34	.7		1.00	1.03
7.7		1.33	1.44	6.9		1.06	1.08
11.3		1.48	1.56	10.5		1.07	1.09
-4.1	.619	1.48	1.61	-4.8	.619	1.02	1.02
1.3		1.77	1.92	.6		1.03	1.03
7.7		2.29	2.36	6.9		1.24	1.24
14.0		2.51	2.51	13.3		1.43	1.60
-3.9	1.300	1.59	1.77	-5.0	1.300	1.00	1.01
1.4		2.03	2.26	.3		1.05	1.06
7.5		3.51	3.82	6.8		1.25	1.30
11.0		2.88	3.22	9.6		1.30	1.52
Measured 12 in. above reference hinge line							
-4.1	0.161	1.07	1.08	-4.7	0.161	1.01	1.02
1.4		1.17	1.21	.7		1.00	1.01
7.7		----	----	6.9		.99	.99
11.3		1.23	1.29	10.5		1.02	1.02
-3.9	1.300	1.22	1.28	-5.0	1.300	1.03	1.04
1.4		1.63	1.76	.3		1.02	1.02
7.5		2.57	2.90	6.8		1.05	1.07
11.0		2.15	2.40	9.6		1.13	1.24

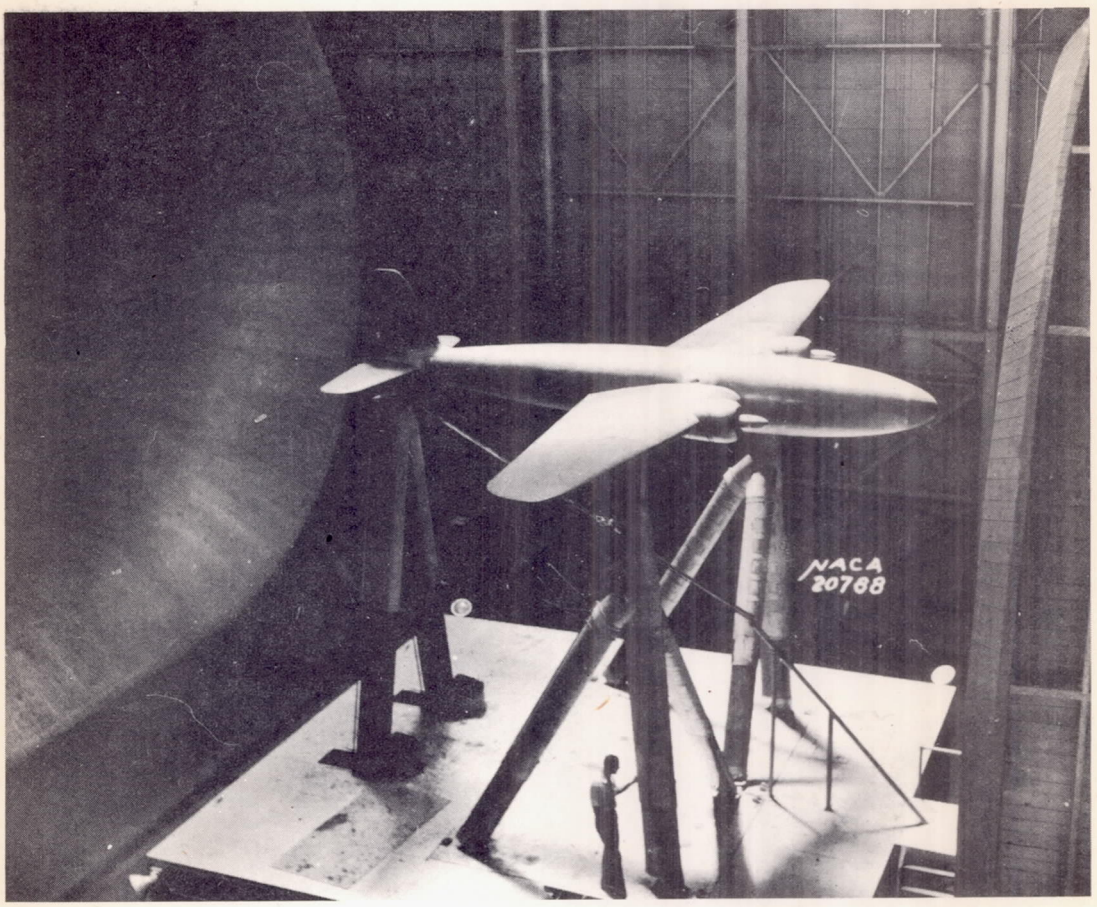

Figure 1.- Installation of stability model in the NACA full-scale wind tunnel.

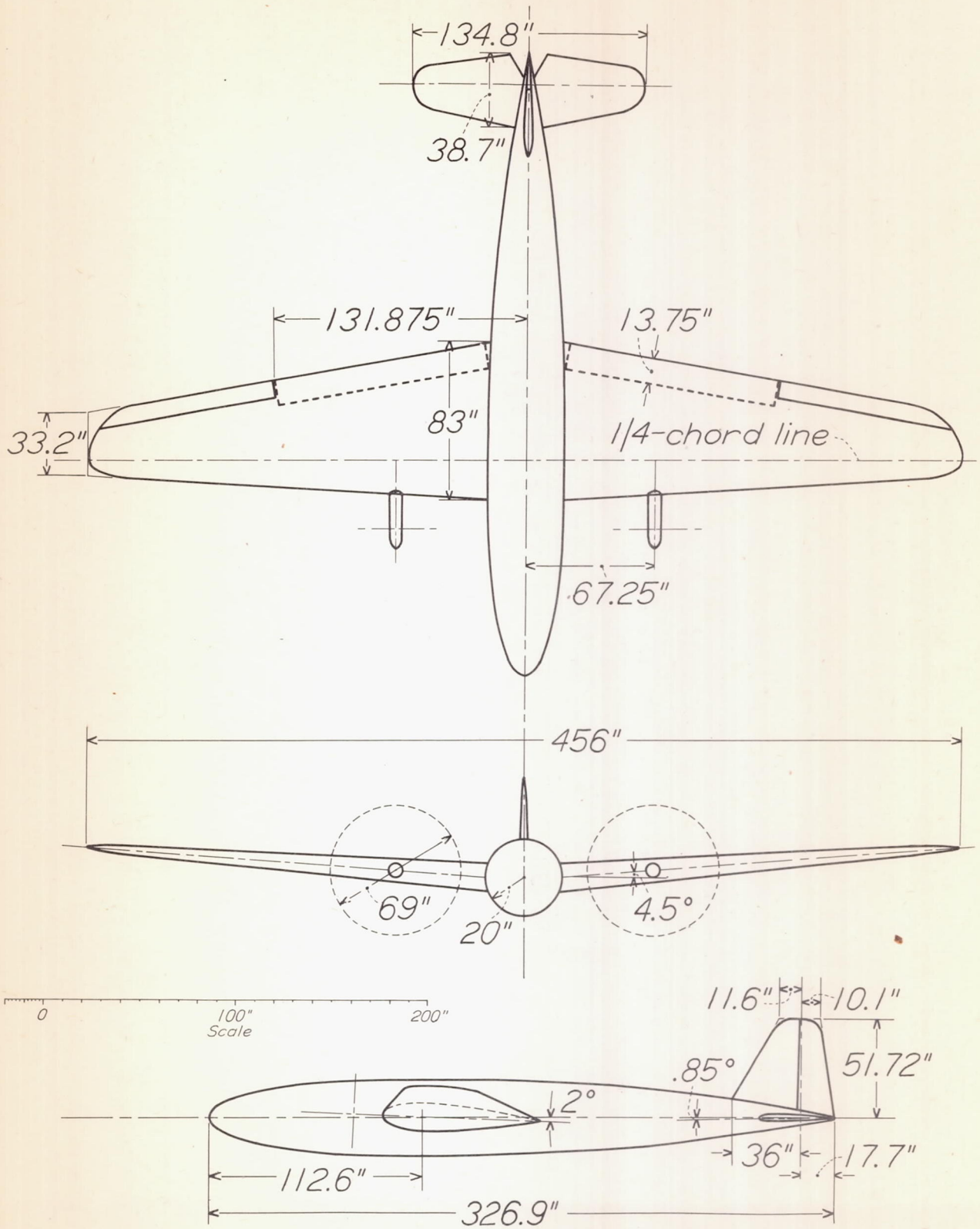

Figure 2.- Three-view drawing of stability model. Nacelles off.

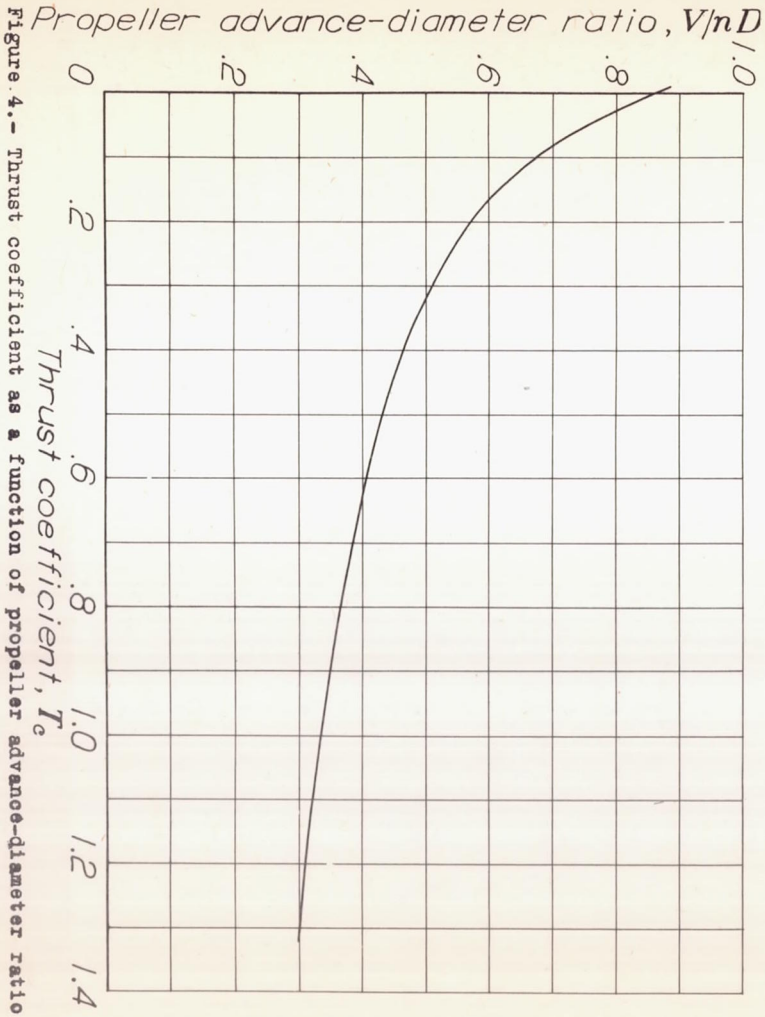

Figure 4.- Thrust coefficient as a function of propeller advance-diameter ratio.

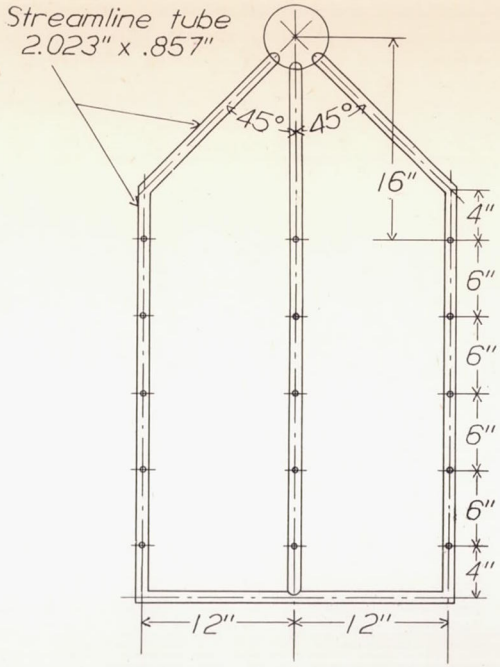

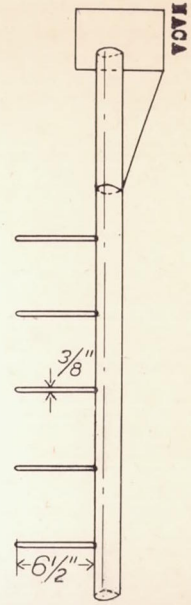

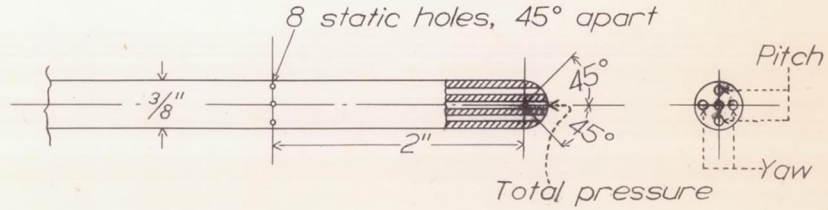

Combined pitch, yaw, and pitot-static tube

Figure 3.- Sketch showing survey rack used to measure the dynamic pressure and the direction of flow of the air stream.

Figs. 3,4

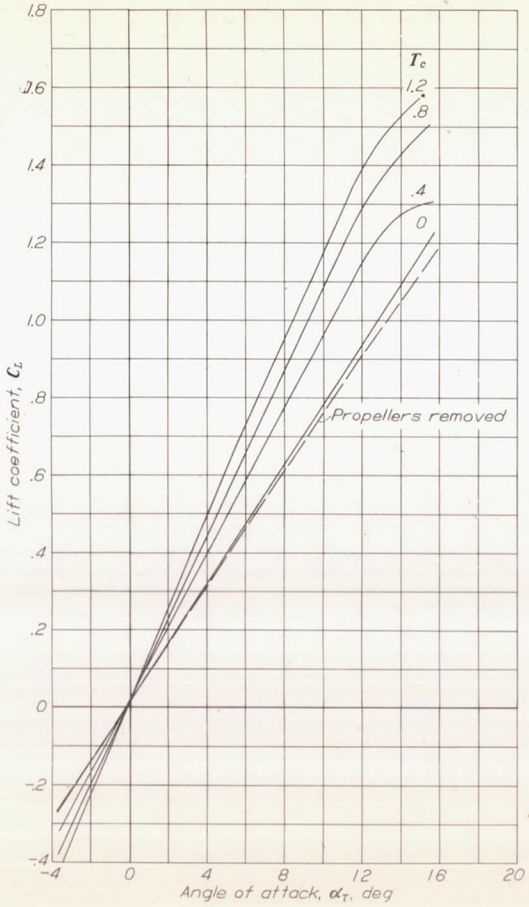

Figure 5.- Effect of propeller operation on model lift coefficient. Flaps retracted; nacelles off; tail off.

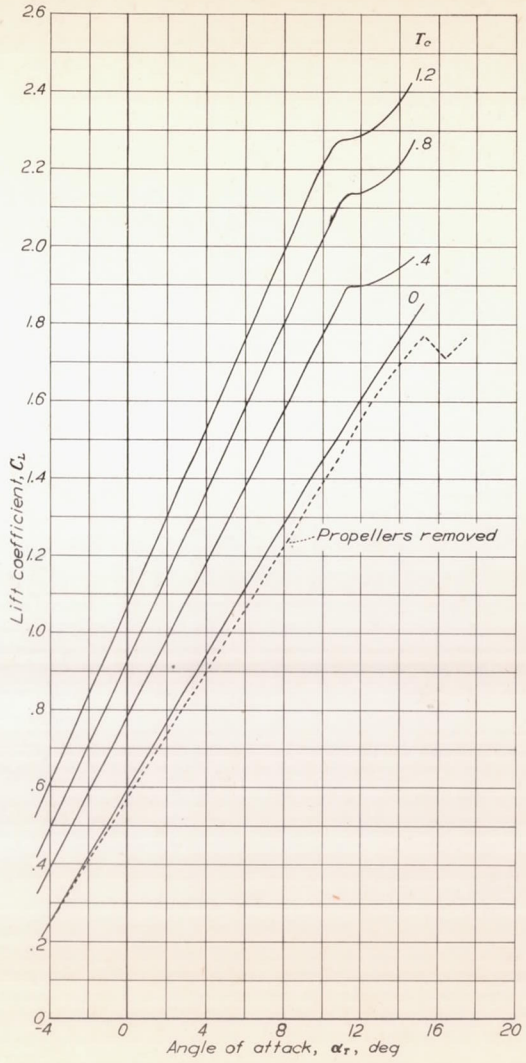

Figure 6.- Effect of propeller operation on model lift coefficient. Flaps deflected 50°; nacelles off; tail off.

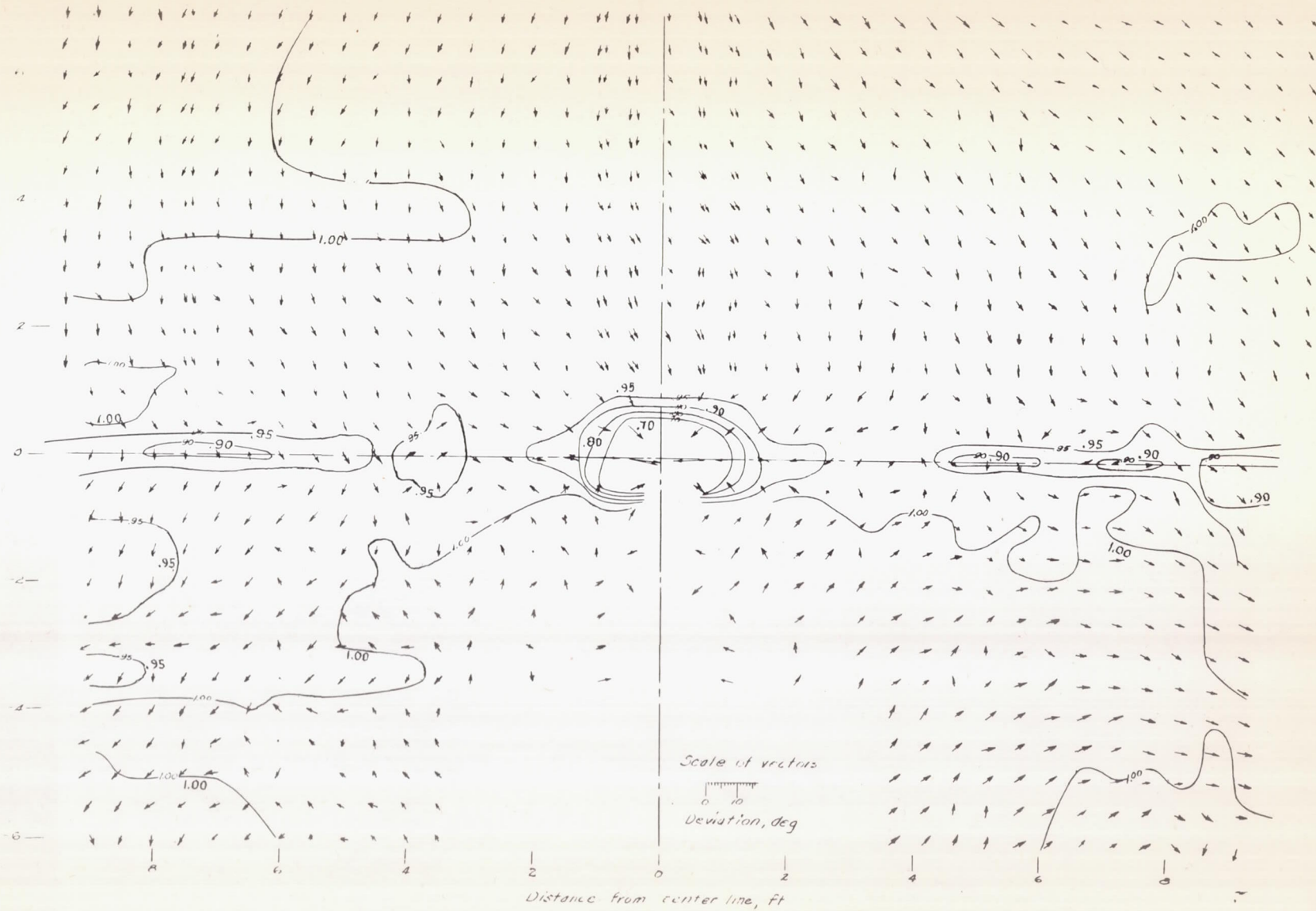

Figure 7 - Dynamic pressure (q/q_0) contours and inclination of the air stream in the plane of the elevator hinge line Vectors show angular deviation of air flow from free-stream direction. View looking forward. Propellers removed; nacelles off flaps retracted.

Fig. 7a

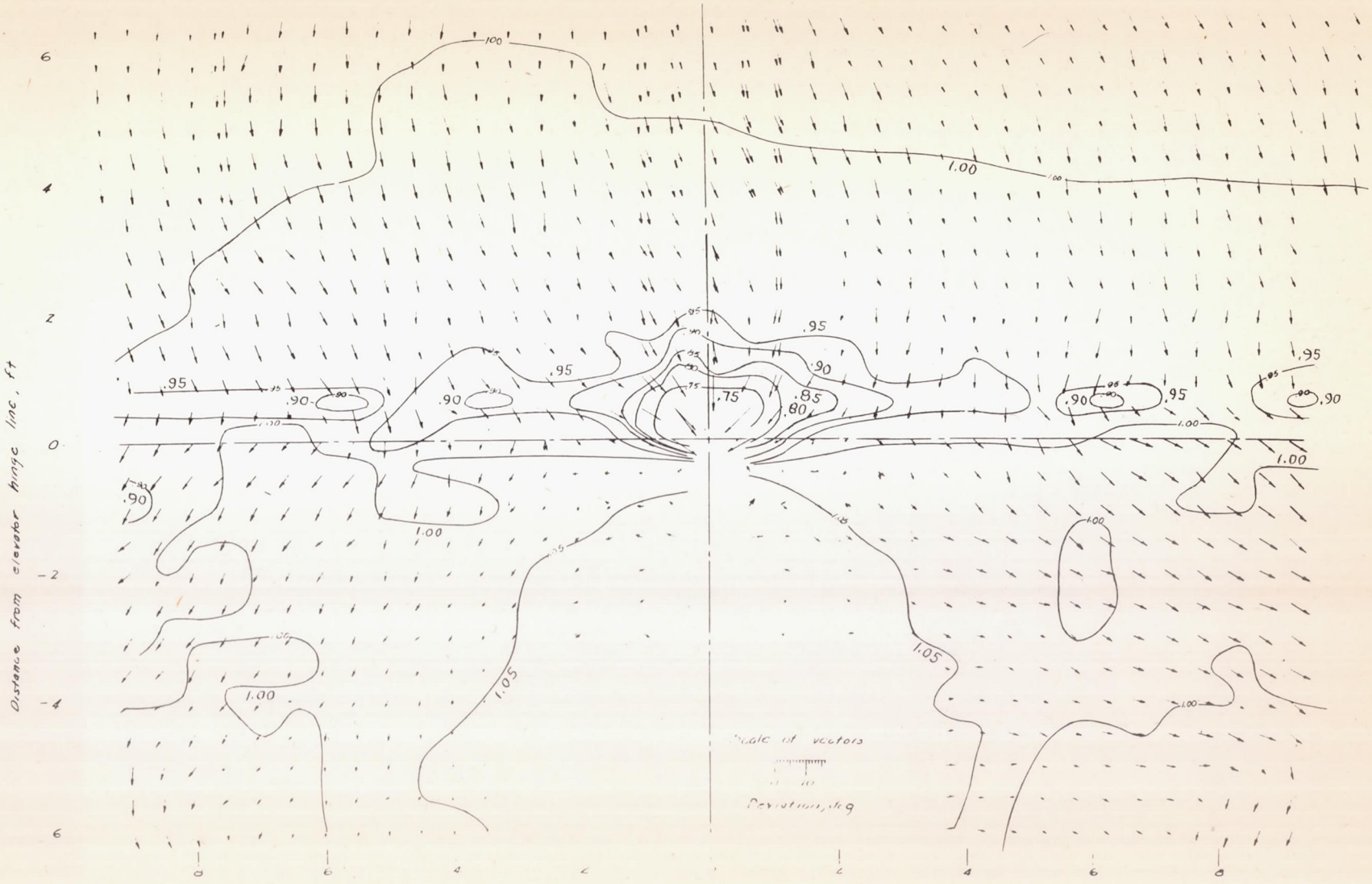

NACA

Fig. 7b

(b) α_T 9.6°

(Figure 7 continued)

(c) α_T 16.0°

Figure 7.- Concluded

Fig. 7c

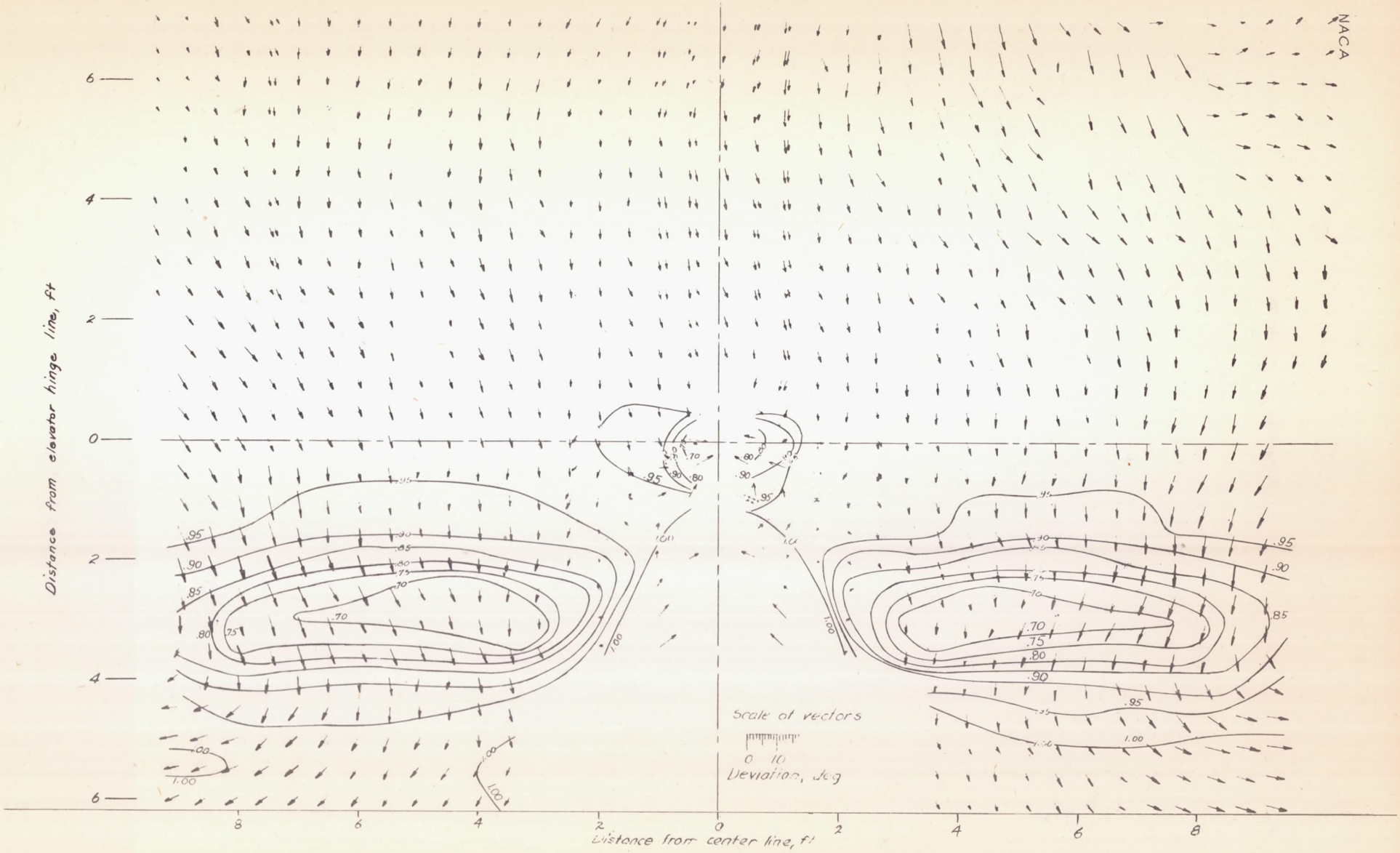

(a) $\alpha_T = -2.7°$

Figure 8.- Dynamic pressure $\left(\frac{q}{q_\infty}\right)$ contours and inclination of the air stream in the plane of the elevator hinge line. Vectors show angular deviation of air flow from free-stream direction. View looking forward. Propellers removed, nacelles off, flaps deflected 50°.

Fig. 8a

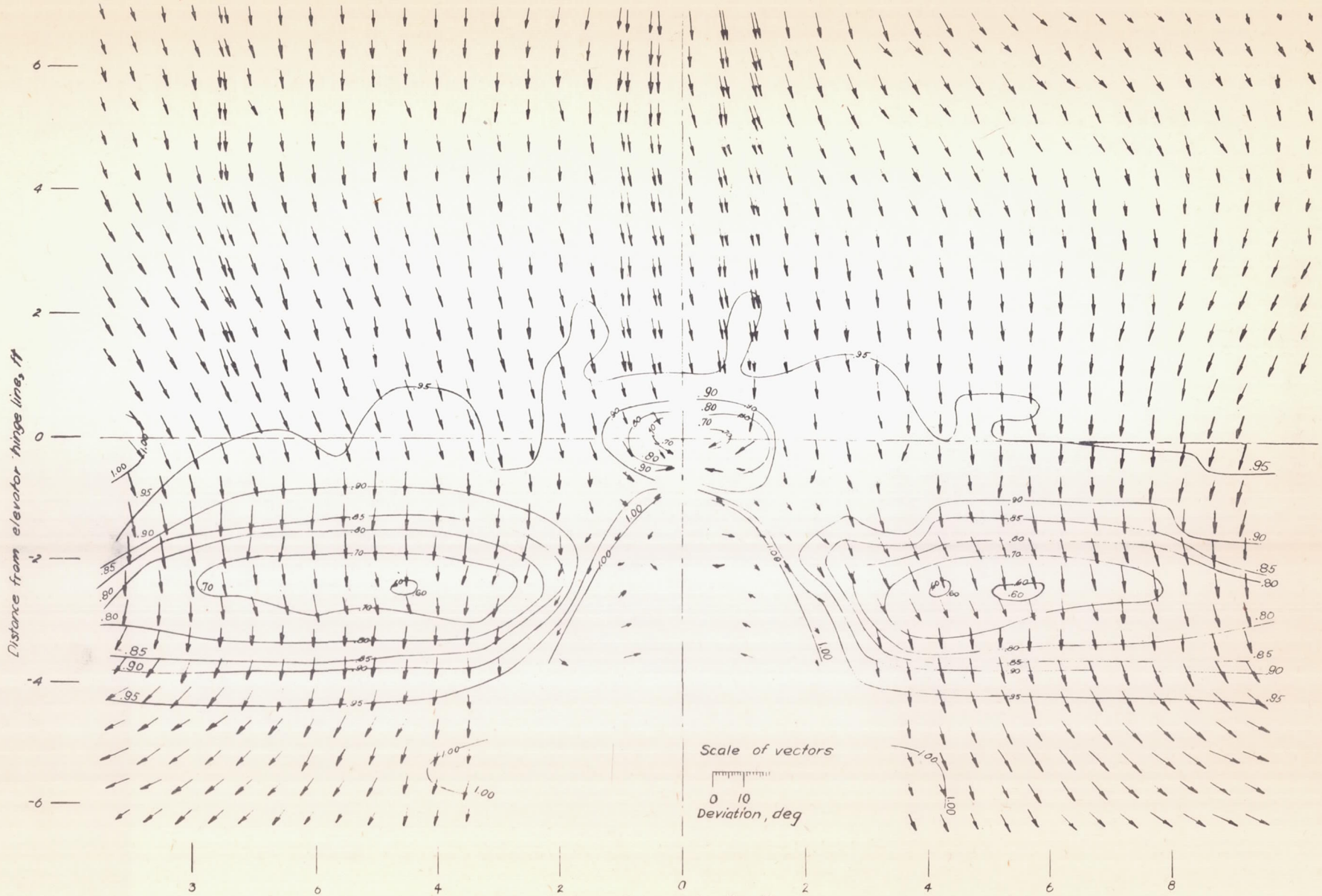

(b) $\alpha_T = 2.7°$

Figure 8.- Continued.

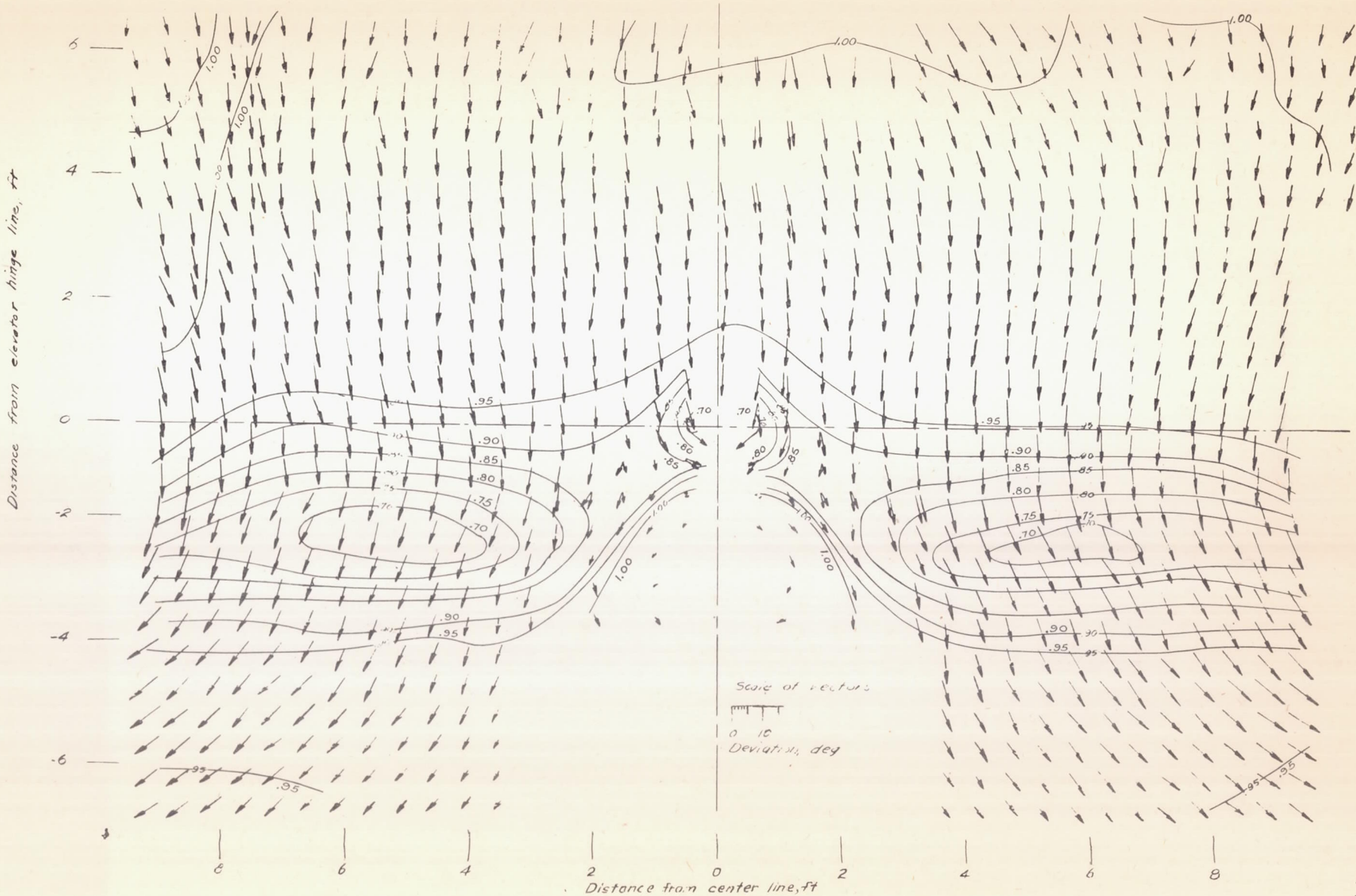

(c) $\alpha_T = 8.9°$

Figure 6.- Continued.

NACA

Fig. 8c

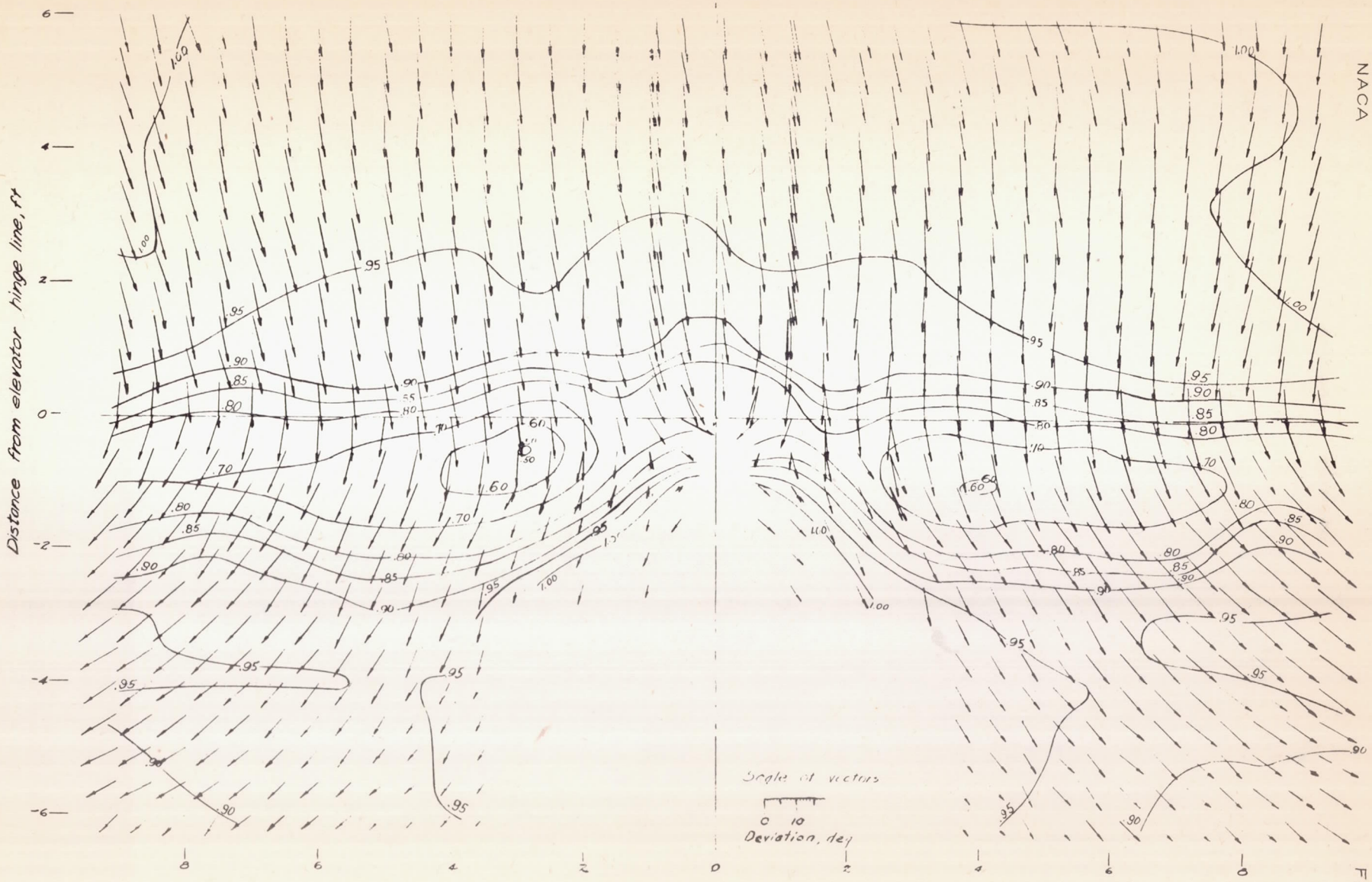

(d) $\alpha_T = 15.2°$

Figure 8.- Concluded.

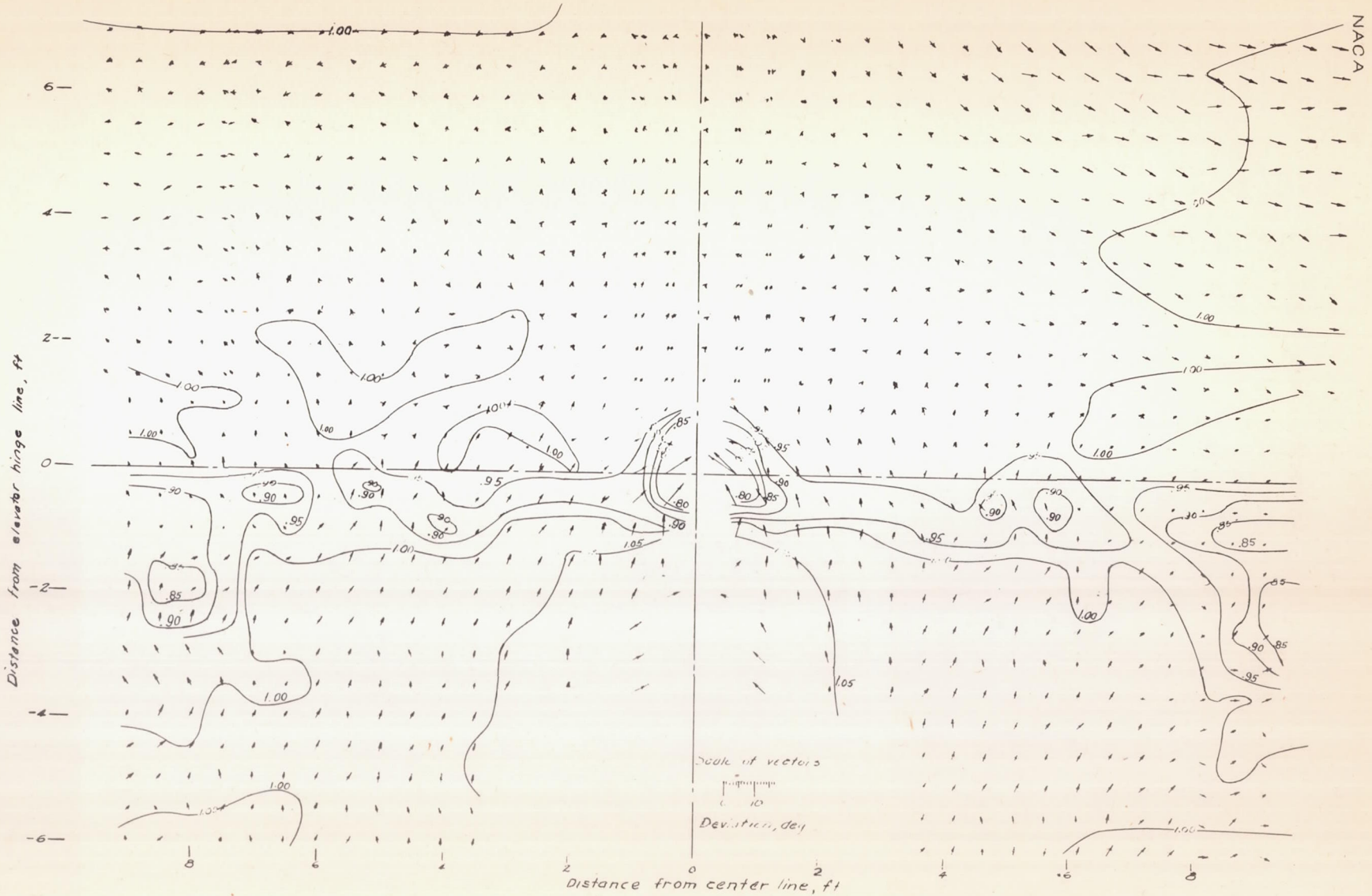

(a) $\alpha_T = -2.3°$

Figure 9.- Dynamic-pressure (q/q_0) contours and inclination of the air stream in the plane of the elevator hinge line. Vectors show angular deviation of air flow from free-stream direction. View looking forward. Propellers removed; nacelles on; flaps retracted.

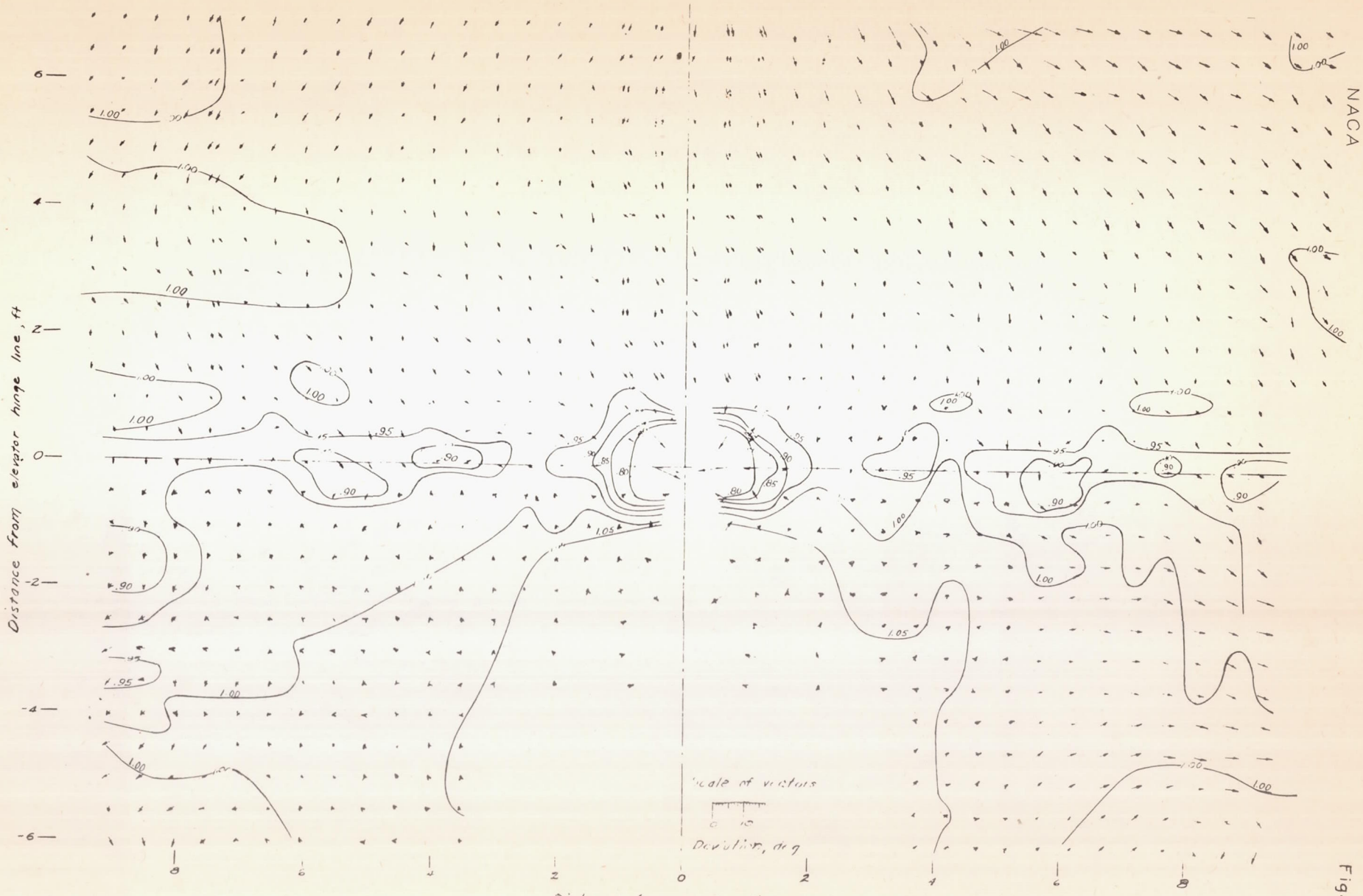

(b) $\alpha_T = 3.2°$

Figure 9 - Continued.

Fig. 9b

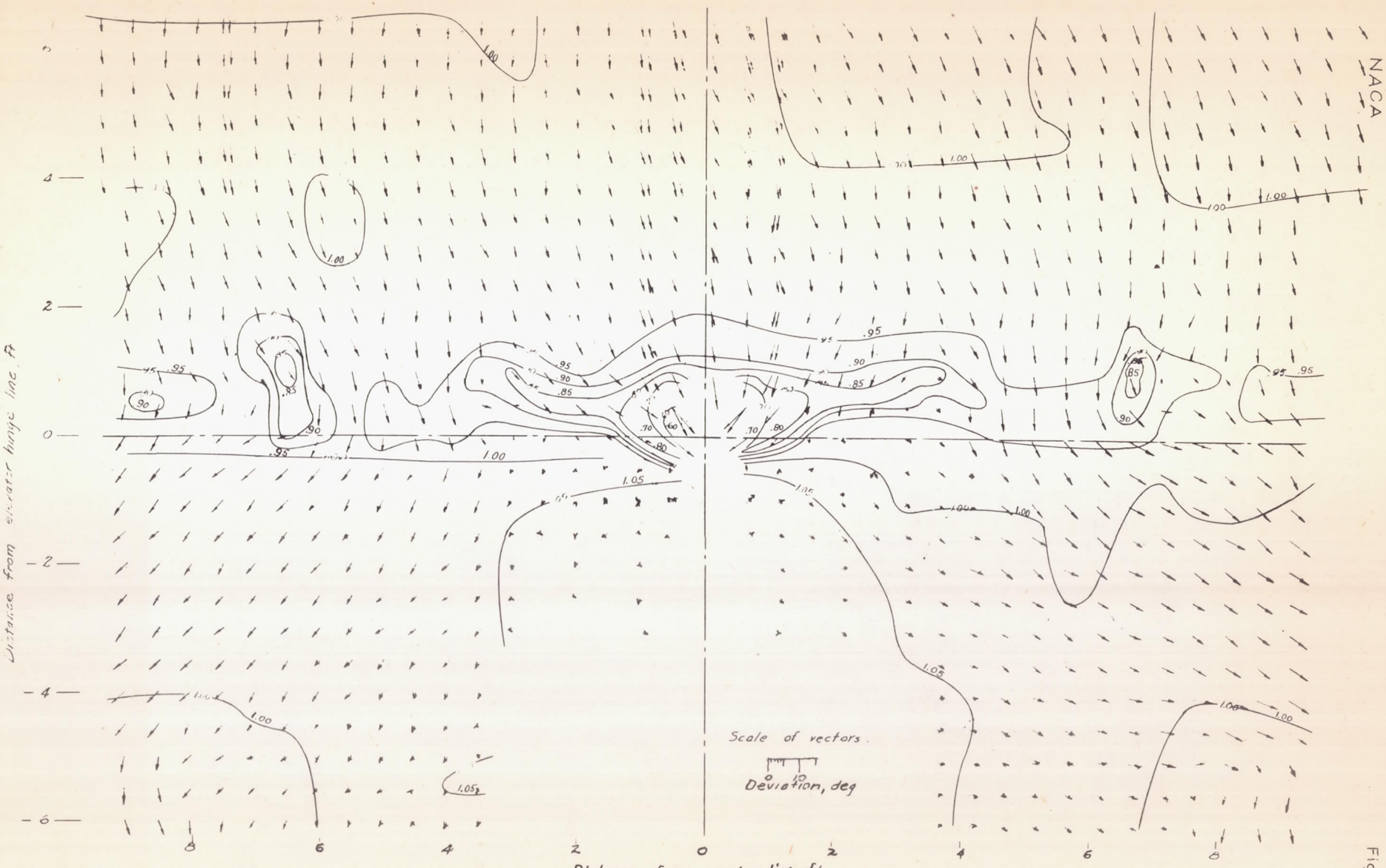

(c) $\alpha_T = 9.6°$

Figure 9 - Continued

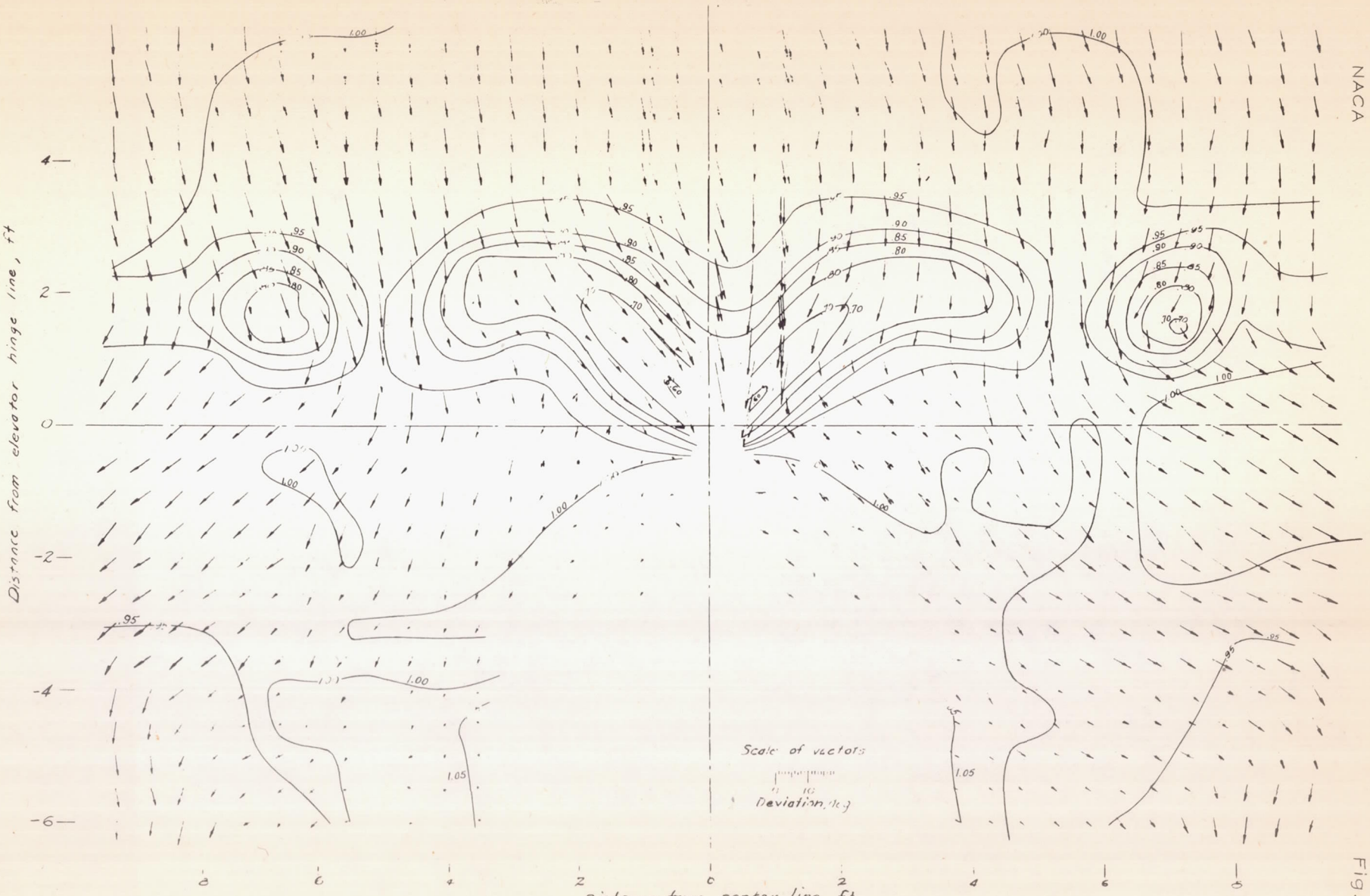

(d) $\alpha_T = 16.0°$

Figure 9.- Concluded.

NACA

Fig. 9d

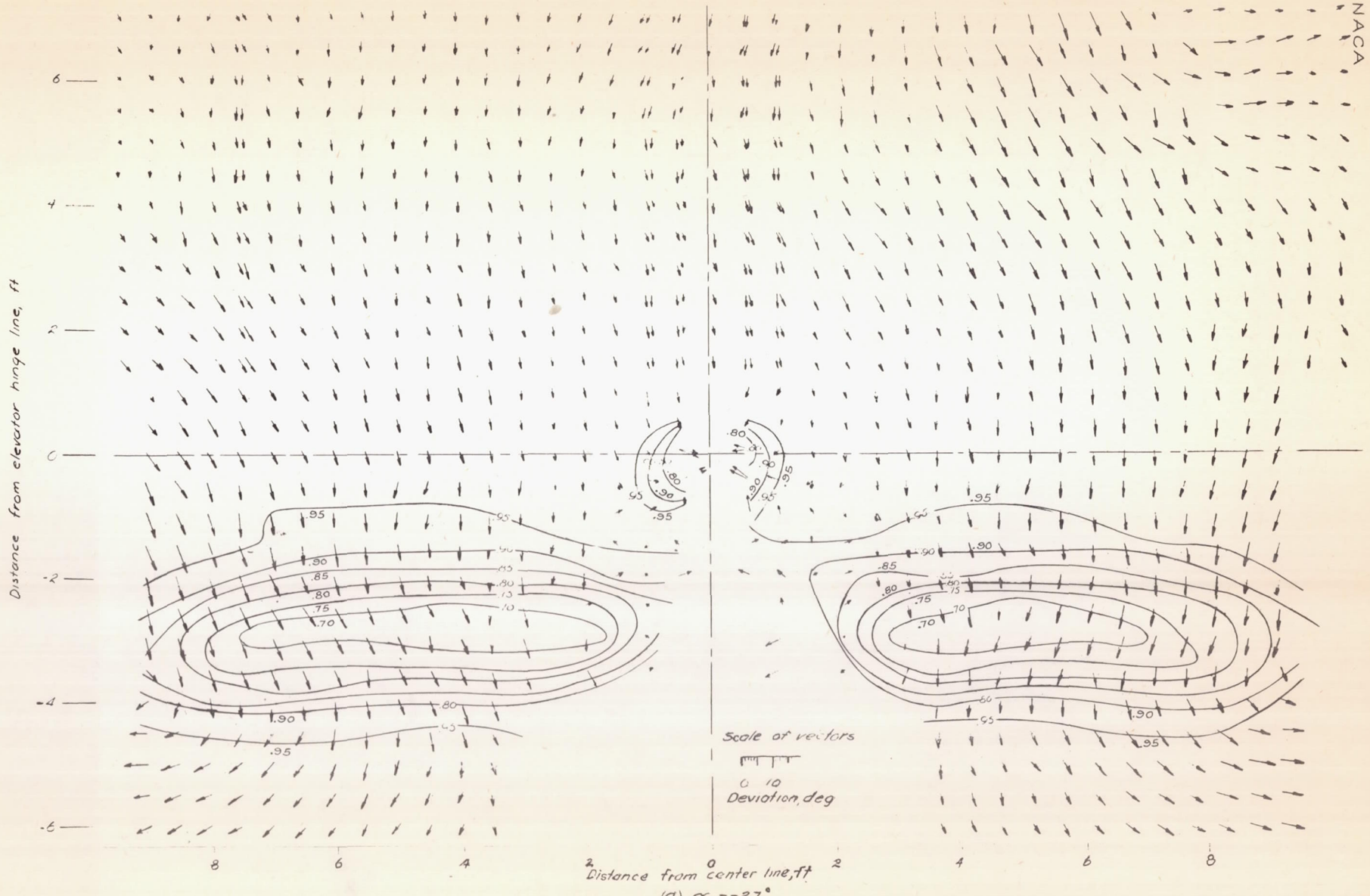

Figure 10.- Dynamic-pressure (q/q_0) contours and inclination of the air stream in the plane of the elevator hinge line. Vectors show angular deviation of air flow from free-stream direction. View looking forward. Propellers removed, nacelles on, flaps deflected 50°.

Fig. 10a

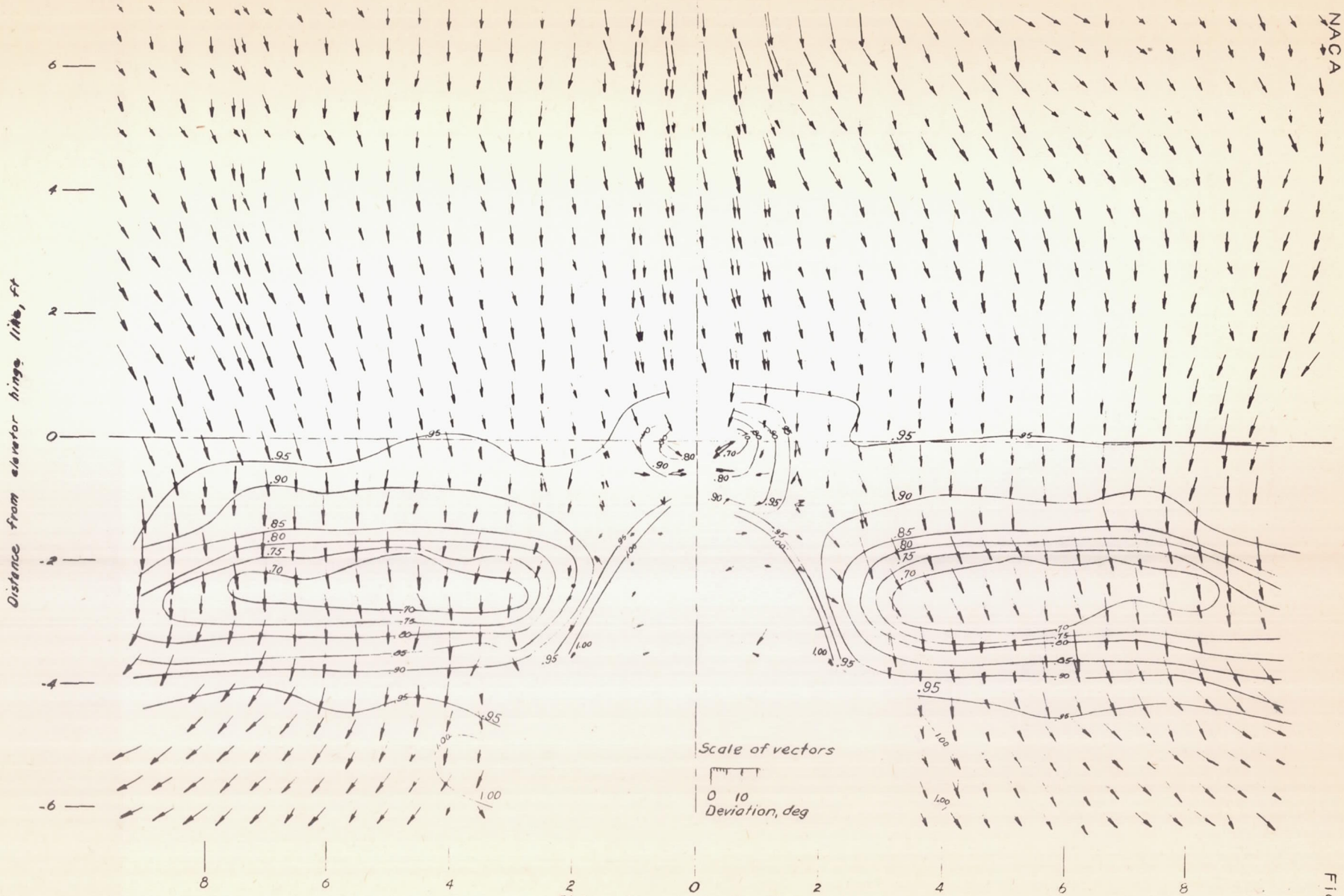

(b) $\alpha_T = 2.7°$

Figure 10.- Continued.

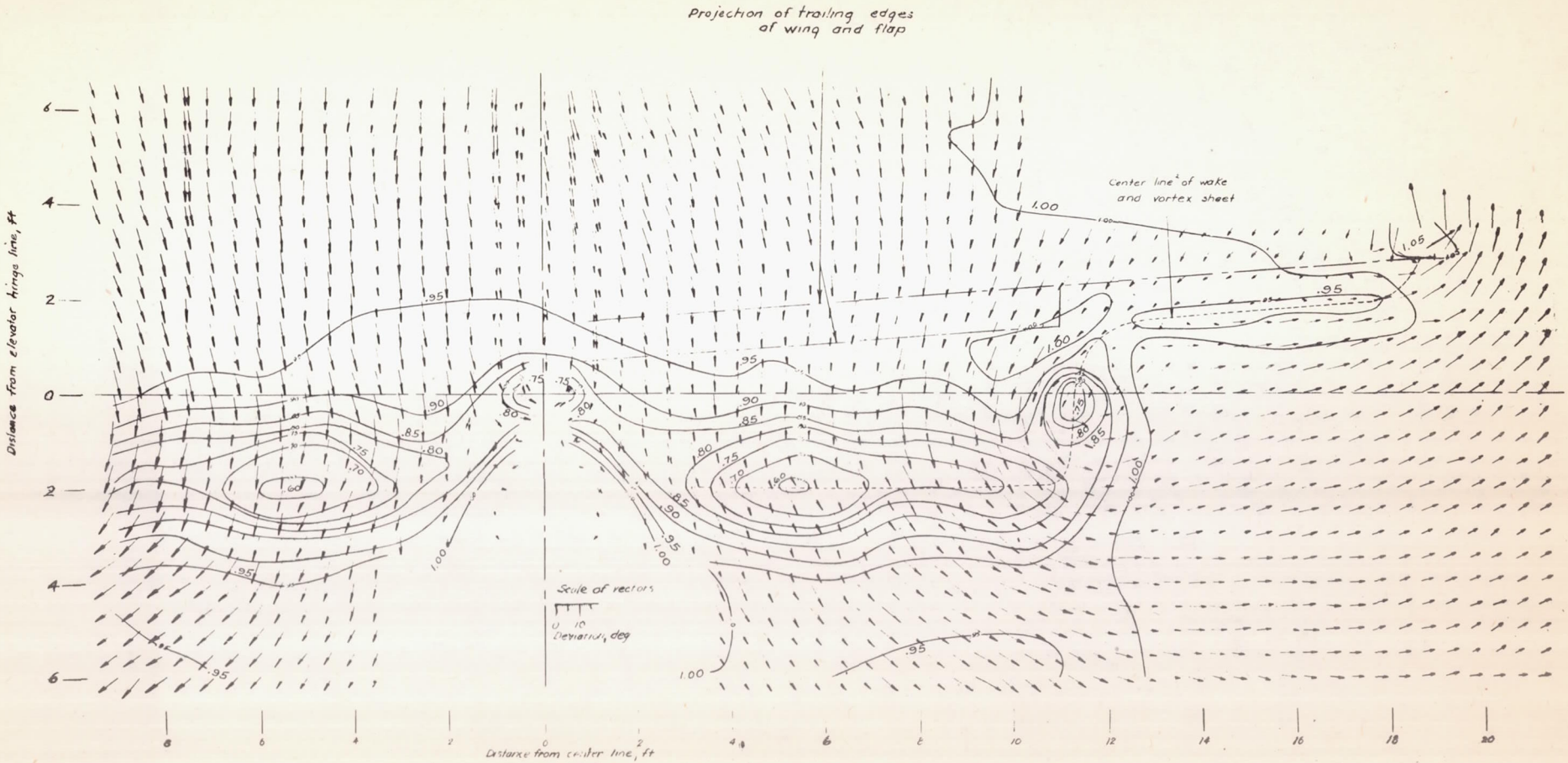

(c) $\alpha_T = 8.9°$

Figure 10.- Continued.

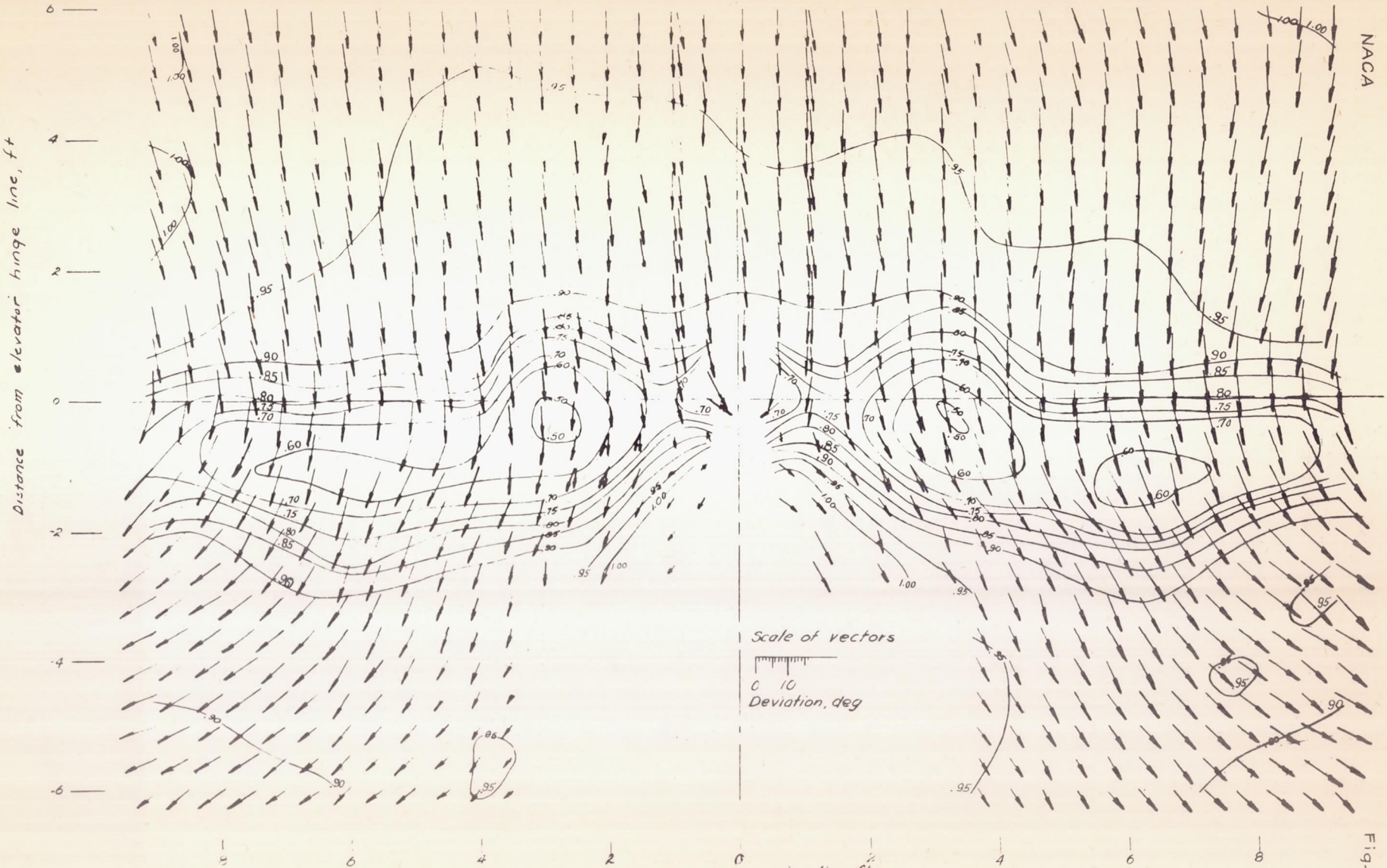

(d) $\alpha_T = 15.2°$.

Figure 10.- Concluded.

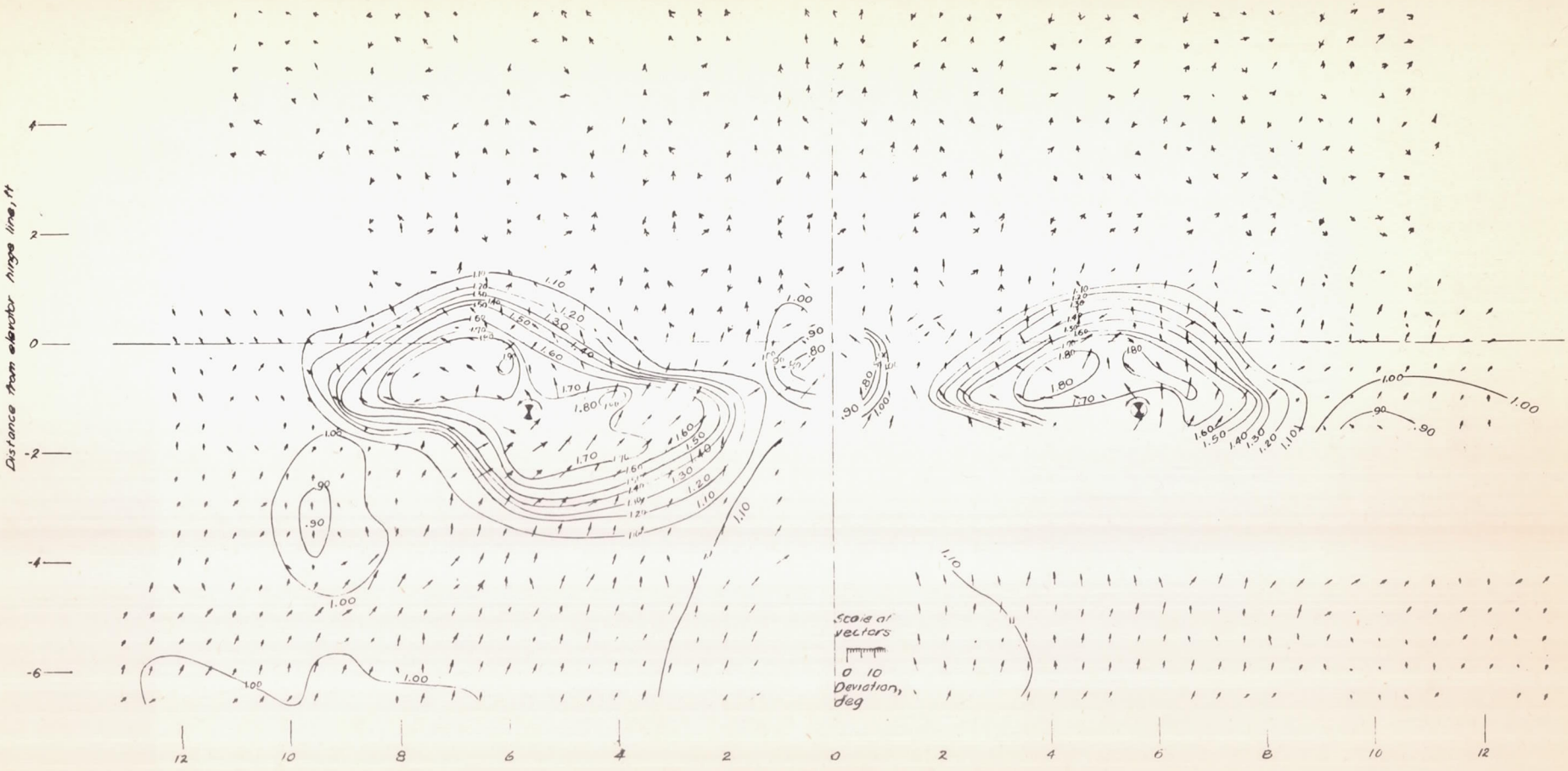

(a) α_T=-4.1°, T_c = 0.161.

Figure 11.- Dynamic-pressure (q/q_0) contours and inclination of the air stream in the plane of the elevator hinge line. Vectors show angular deviation of air flow from free-stream direction. View looking forward. Circles show projection of propeller centers Nacelles off flaps retracted.

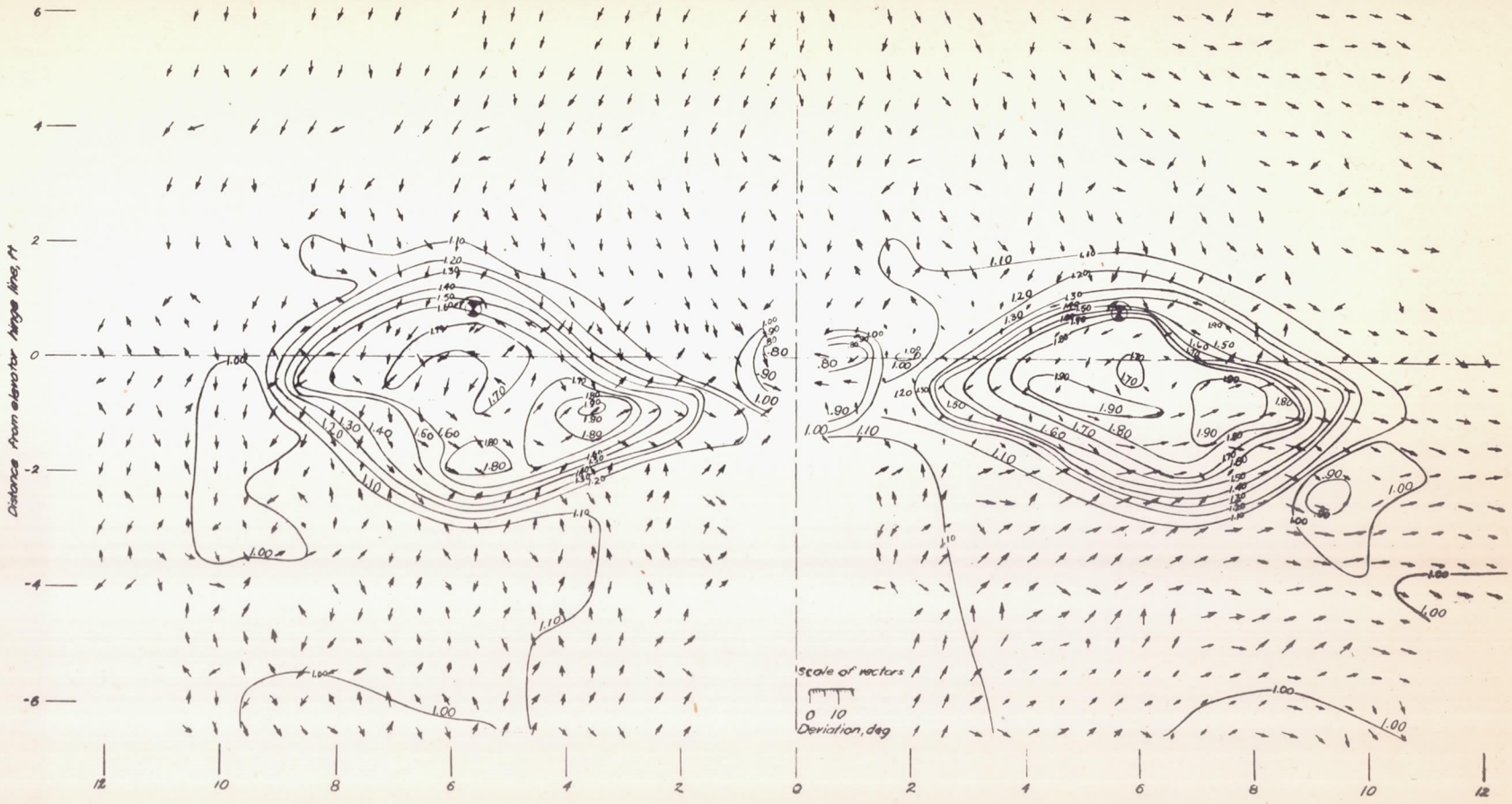

(b) $\alpha_T = 1.4°$; $T_c = 0.161$.

Figure 11.- Continued.

NACA

Fig. 11c

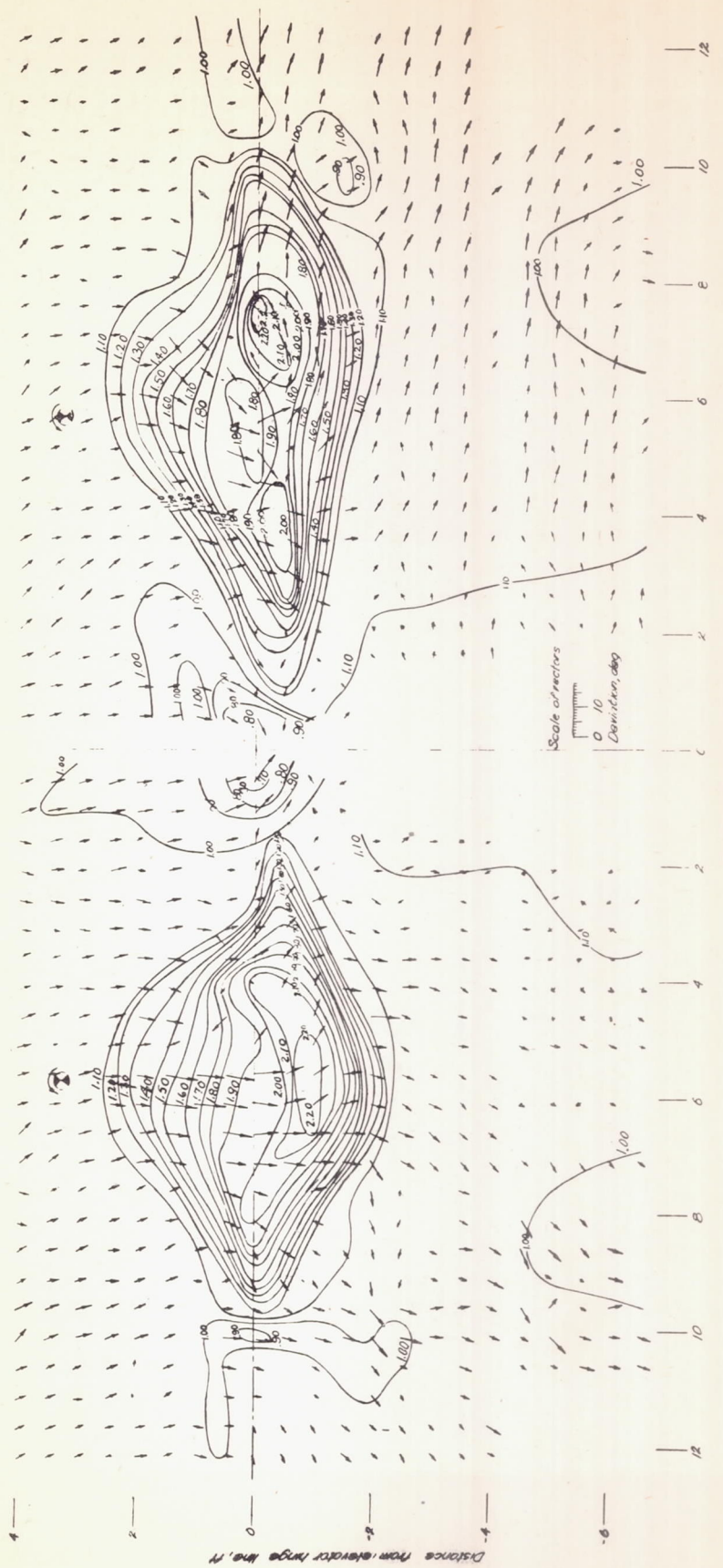

(c) $\alpha_T = 7.7°$; $\bar{c}_c = 0.161$.

Figure 11.- Continued.

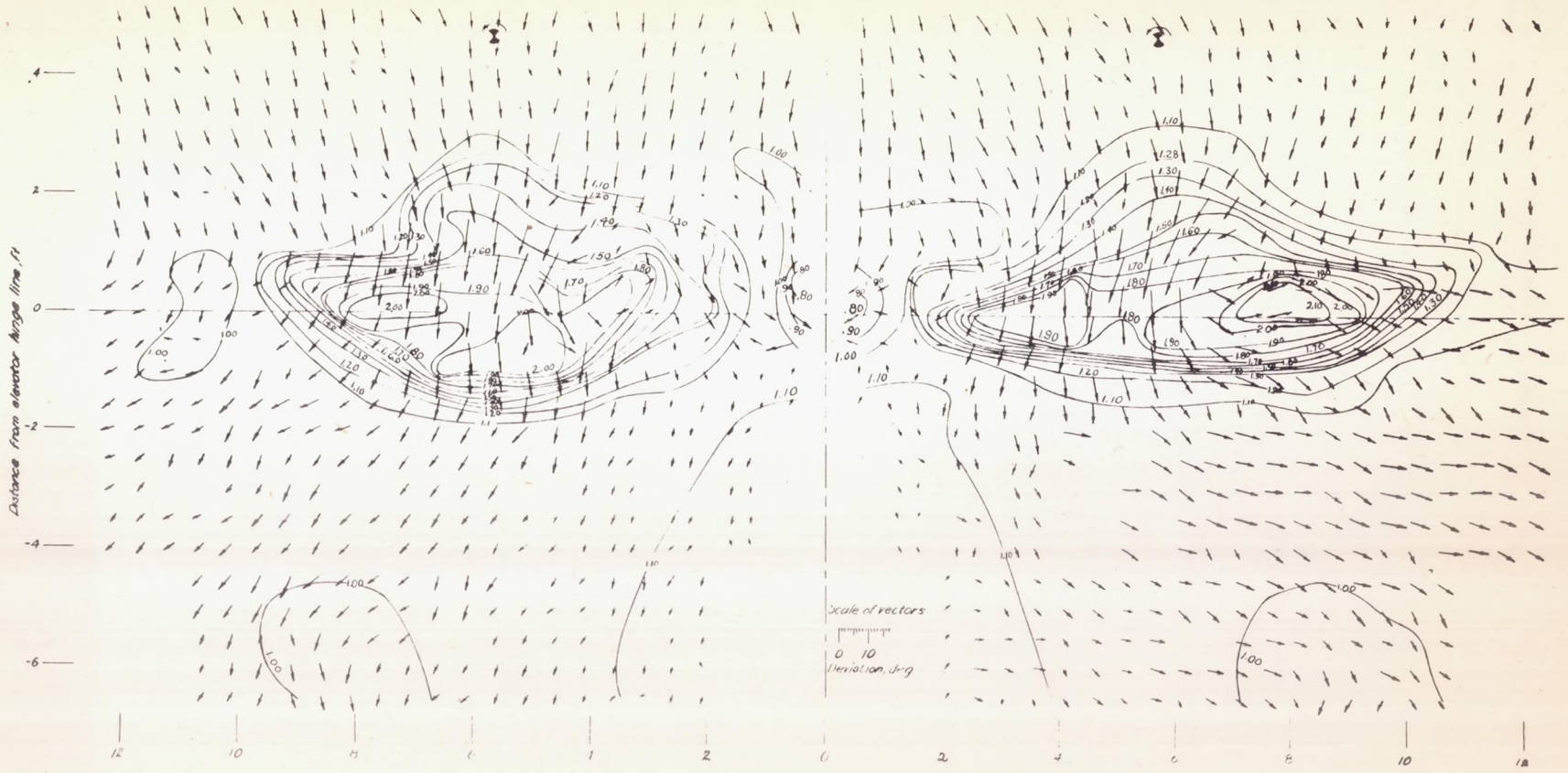

(d) $\alpha_r = 14.1°$; $T_c = 0.161$

Figure 11.- Continued.

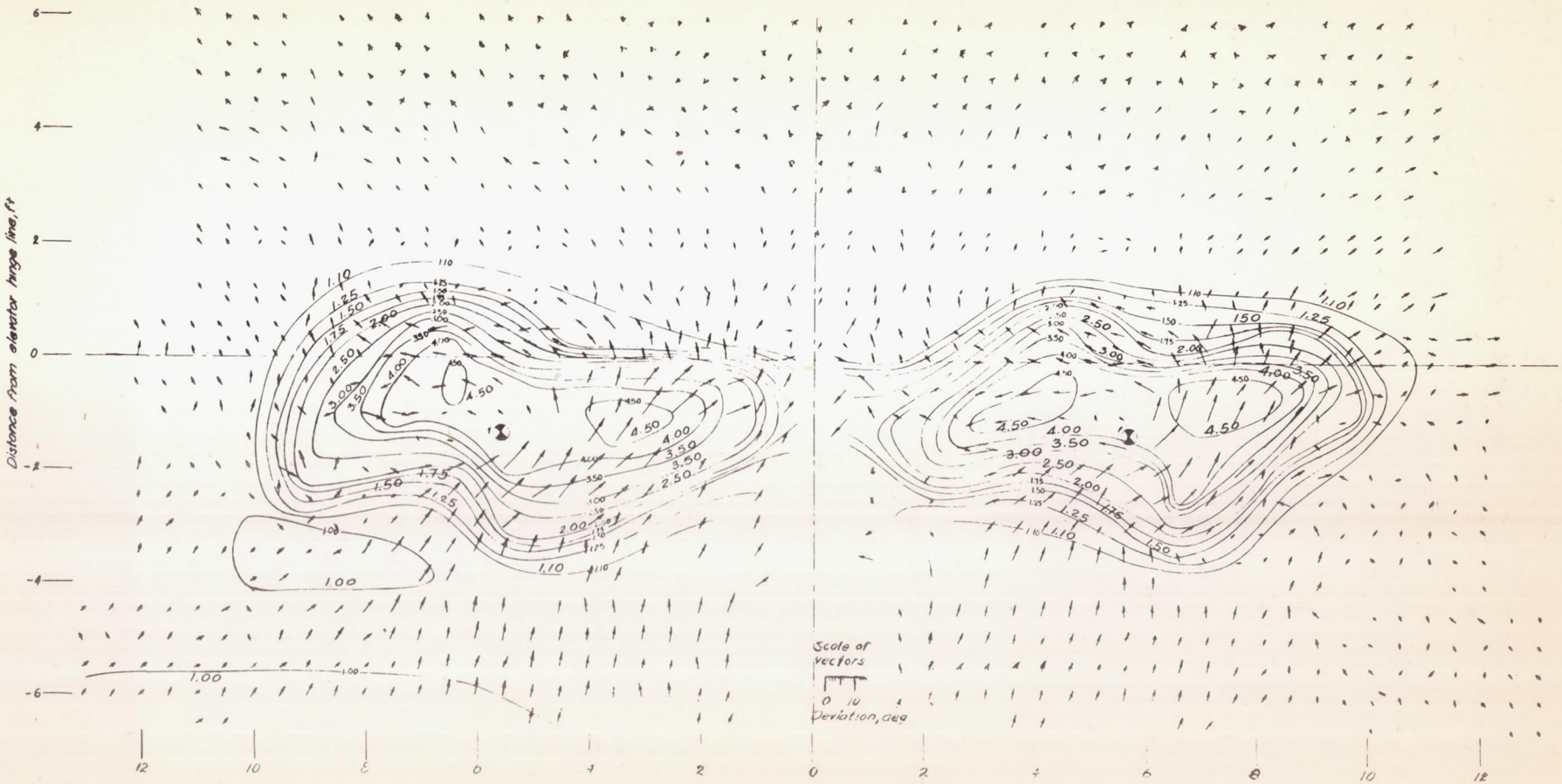

(e) $\alpha_T = -39°$; $T_c = 1.300$.

Figure 11.- Continued.

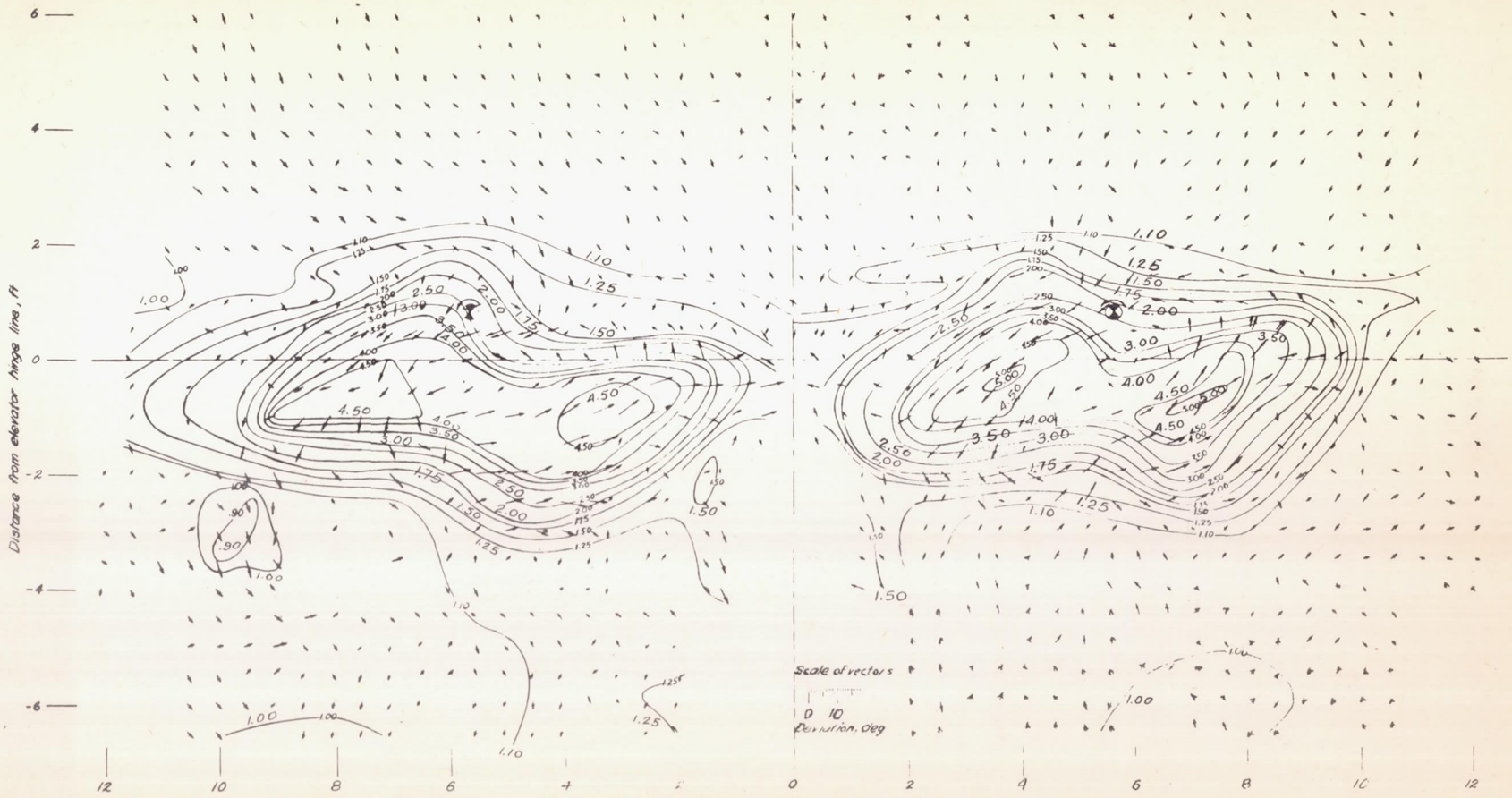

(f) $\alpha_T = 1.4°$ $T_C = 1.300$.

Figure 11. Continued.

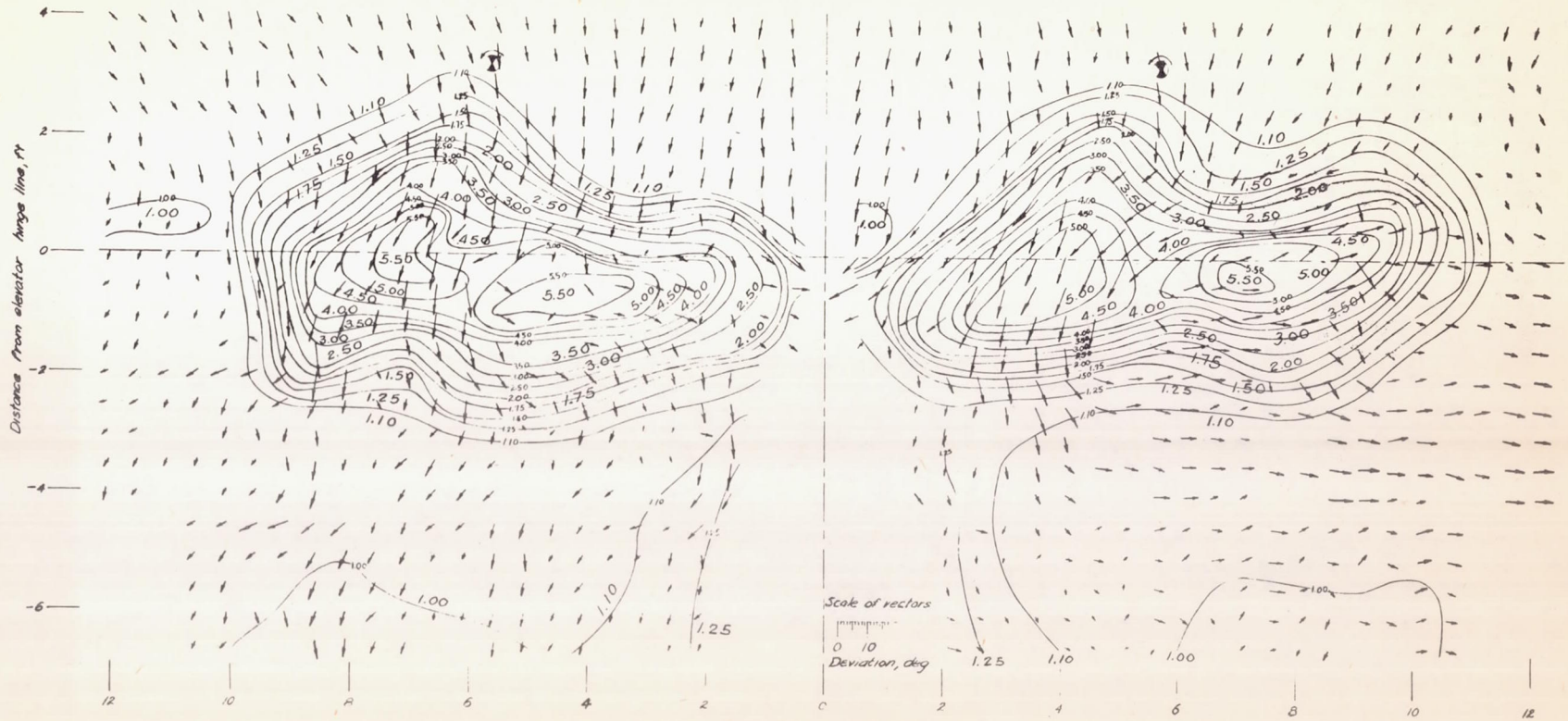

(g) α_T 7.5°; T_c = 1.300

Figure 11 - Continued.

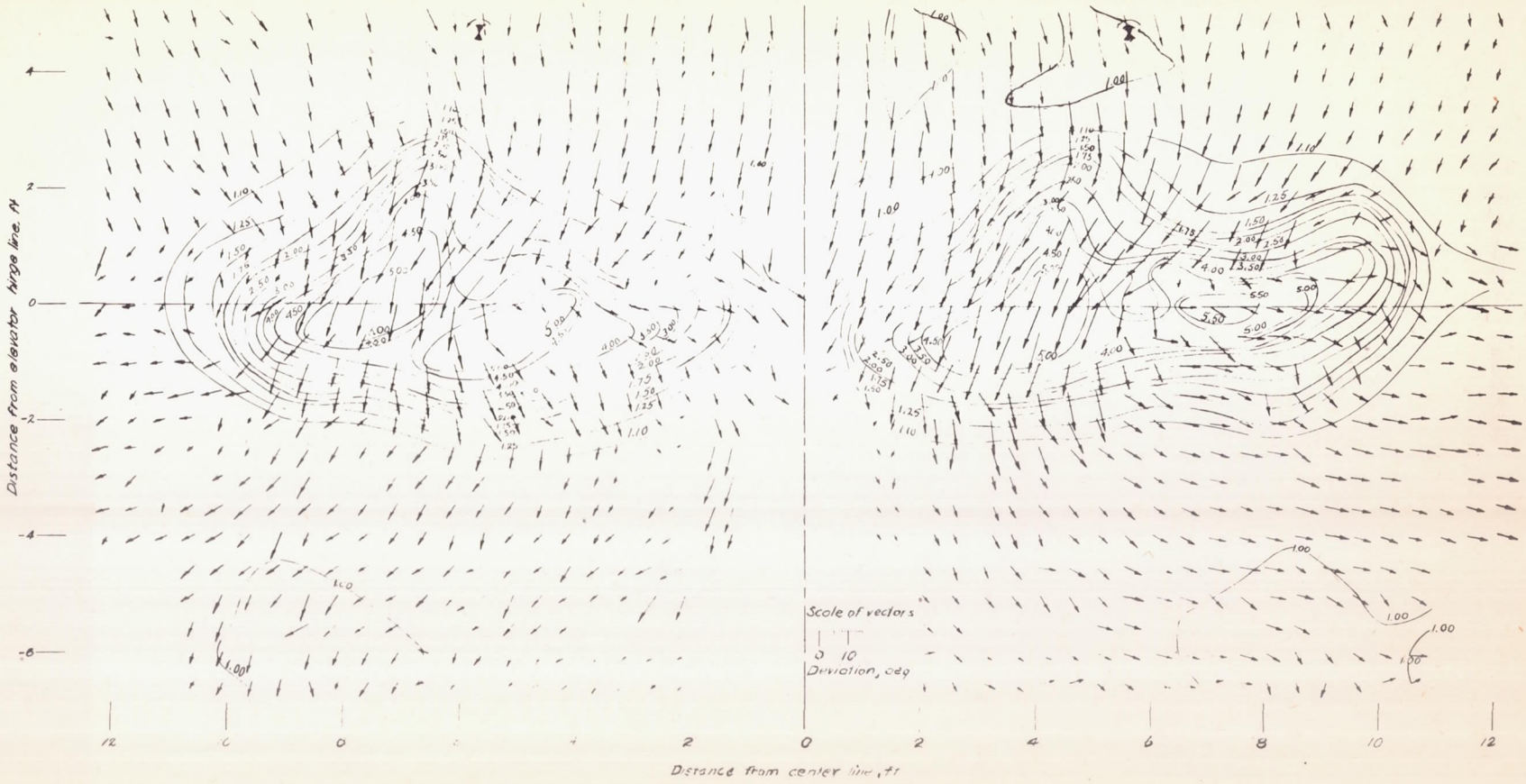

(h) $\alpha_r = 11.0°$; $T_c = 1,300$

Figure 11.- Concluded.

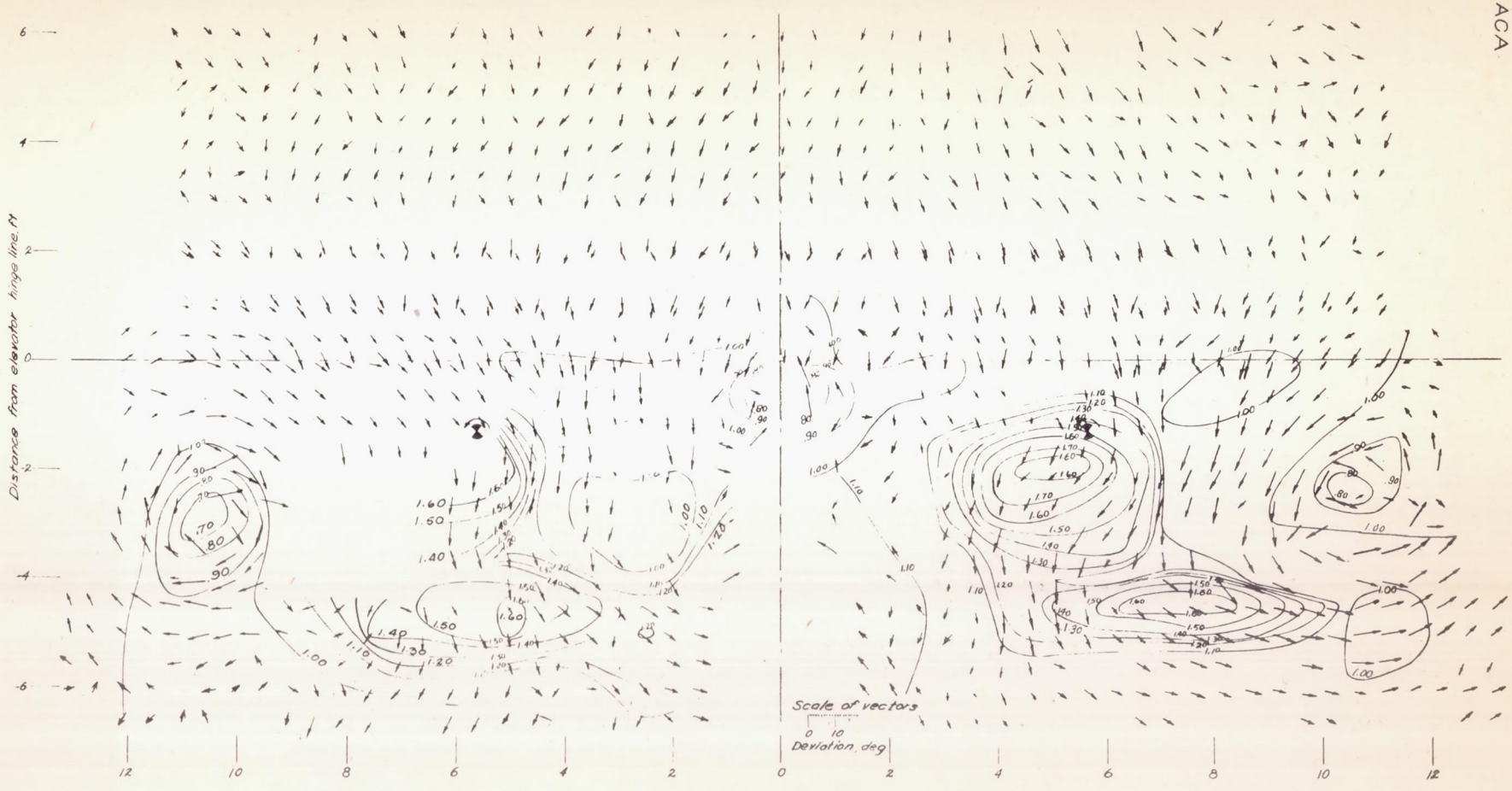

(a) $\alpha_T = -4.7°$; $T_C = 0.161$.

Figure 12.- Dynamic-pressure (q/q_0) contours and inclination of the air stream in the plane of the elevator hinge line. Vectors show angular deviation of air flow from free-stream direction. View looking forward. Circles show projection of propeller centers. Nacelles off, flaps deflected 50°.

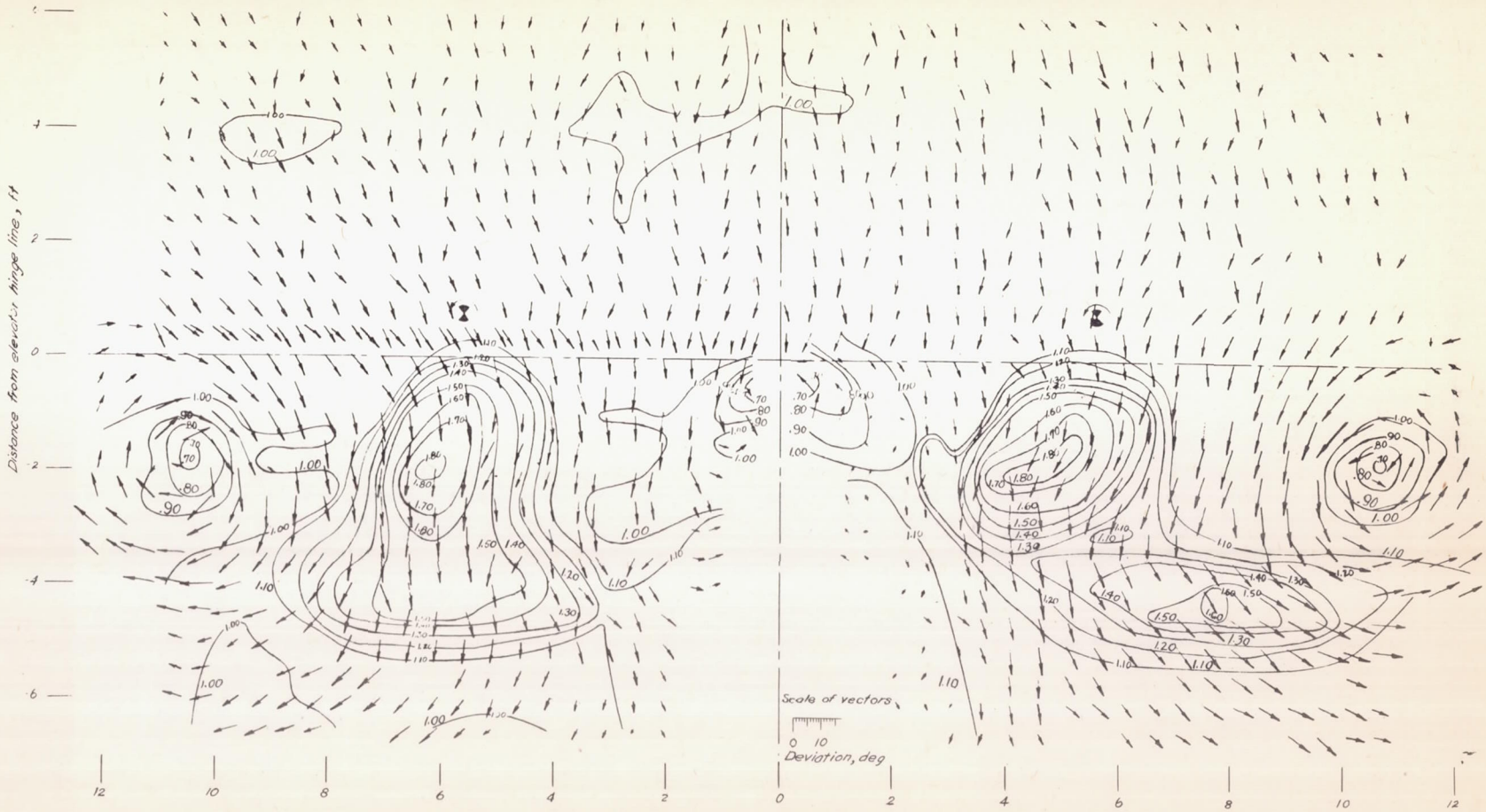

(b) $\alpha_T = 0.1°_j$ $T_c = 0.161$

Figure 12.- Continued.

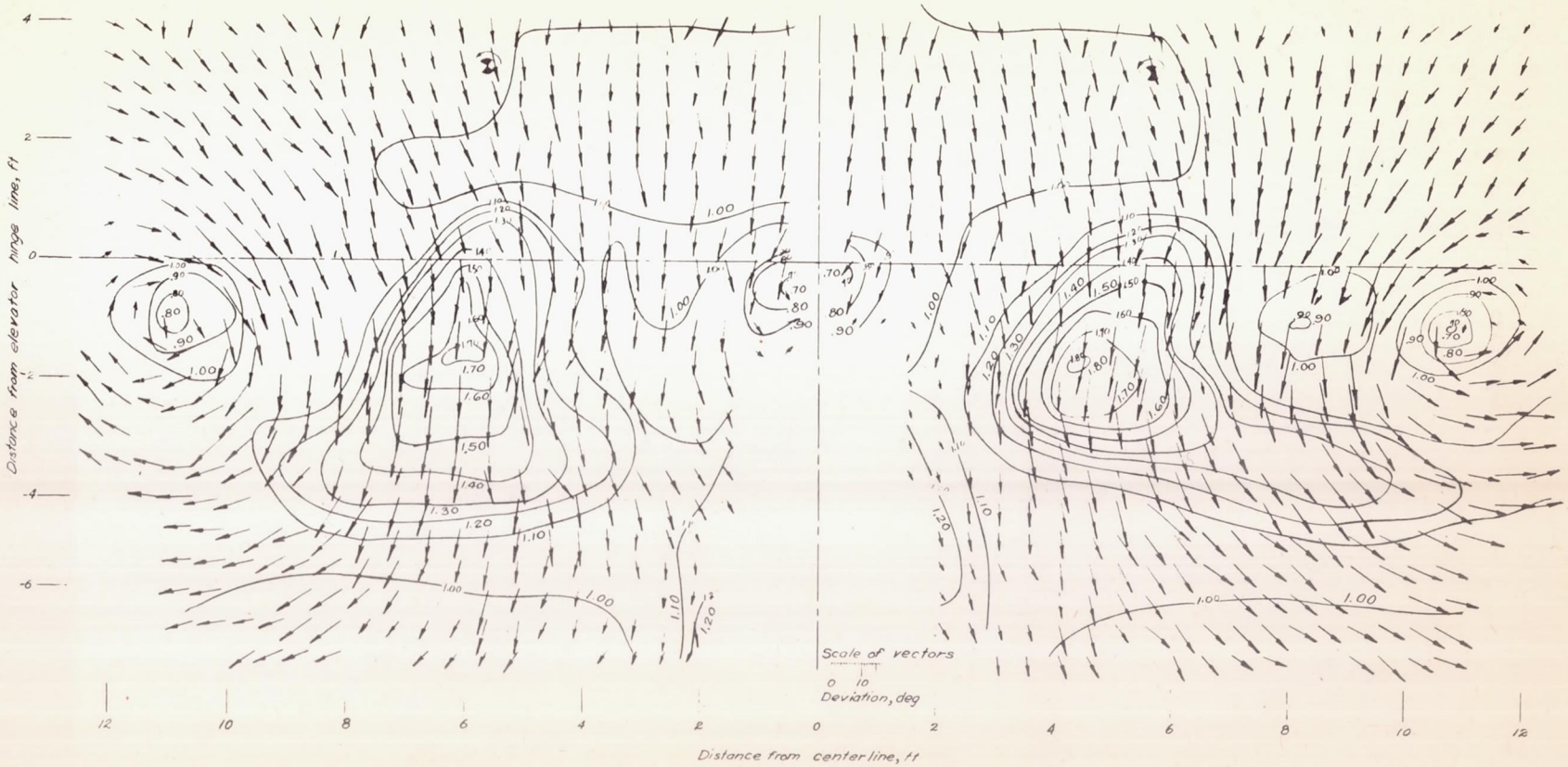

(c) $\alpha_T = 6.9$; $T_C = 0.161$.

Figure 12.- Continued.

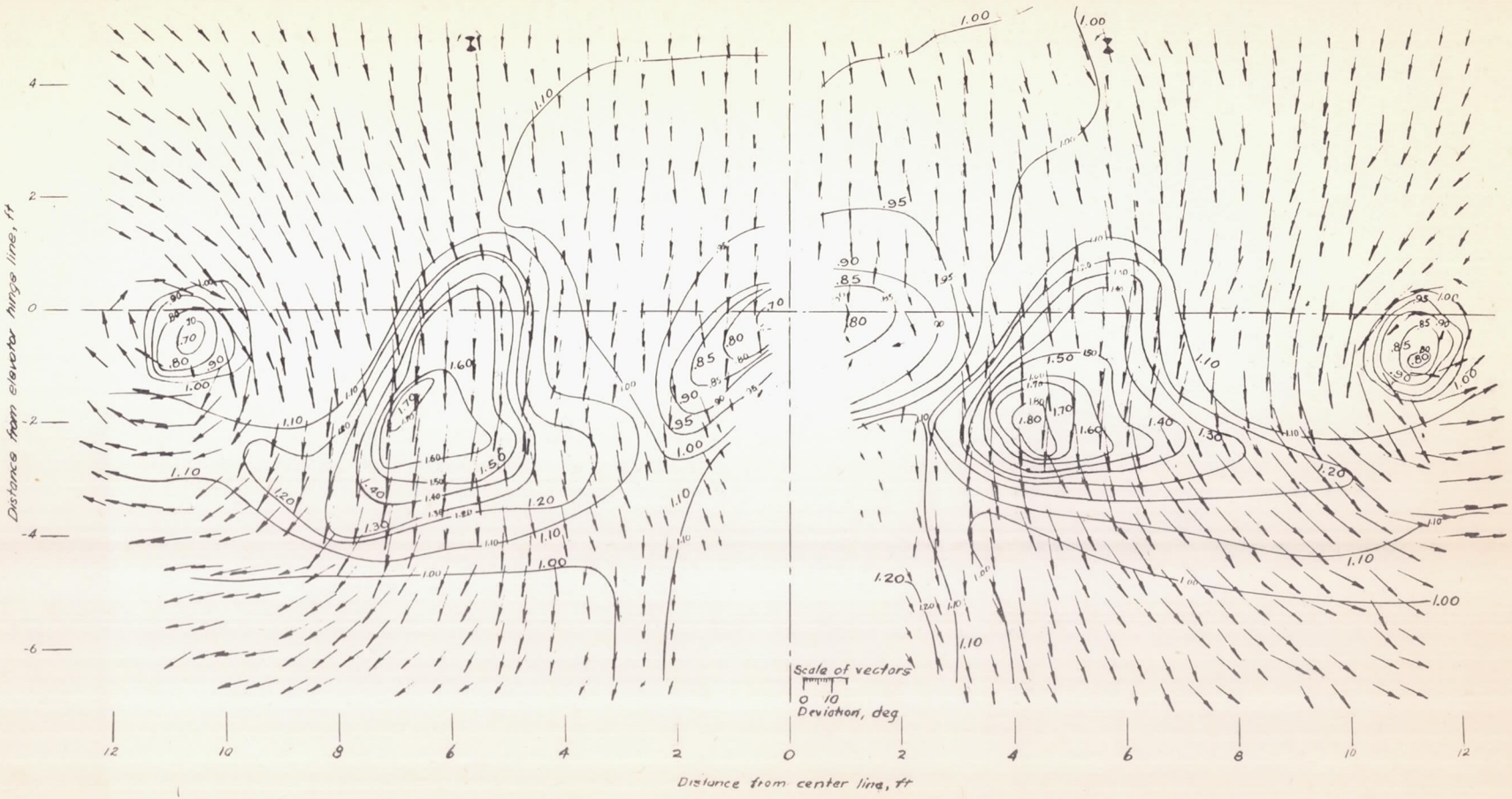

(d) $\alpha_T = 10.5°$; $T_c = 0.161$.

Figure 12. Continued.

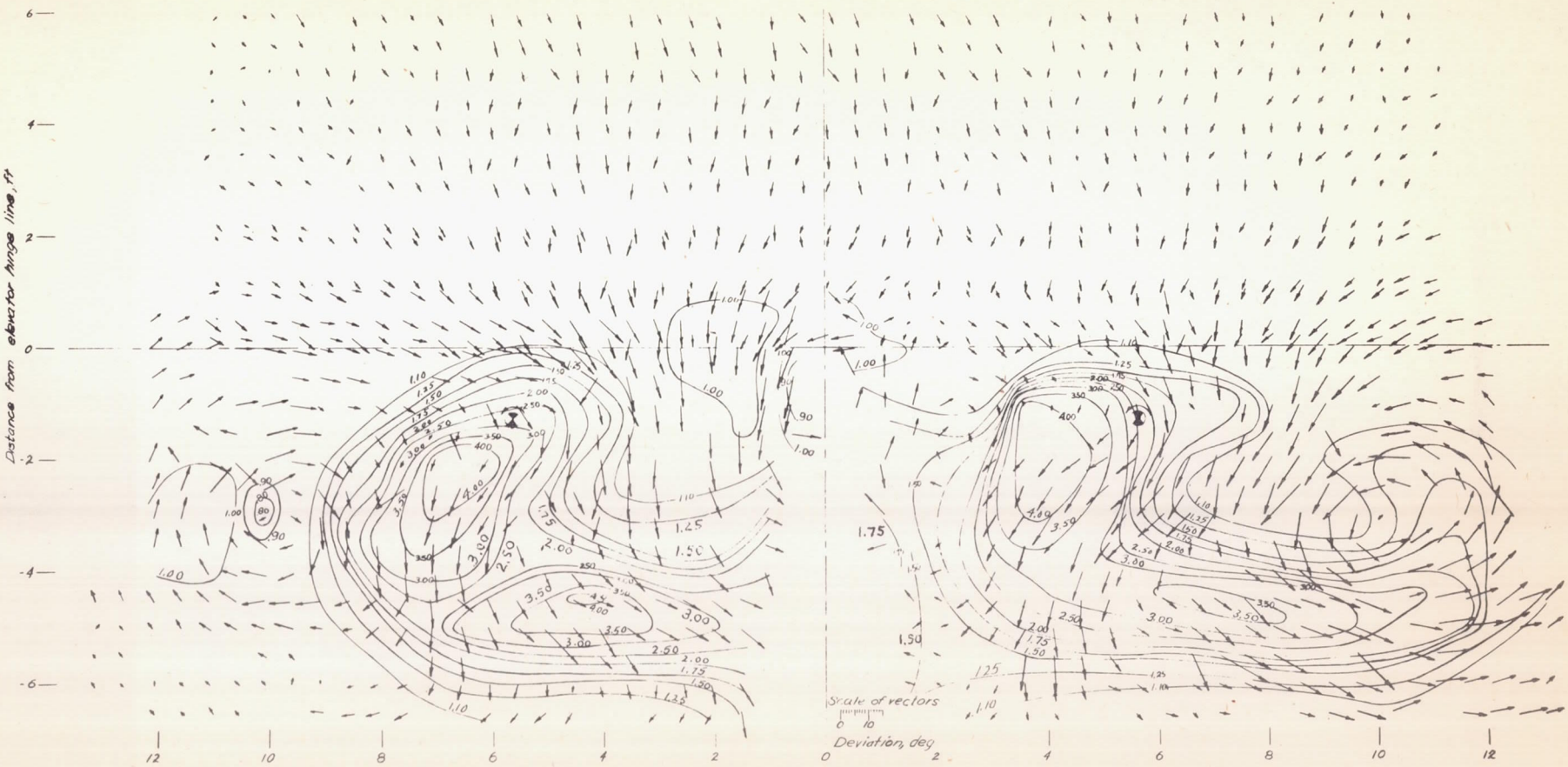

(e) $\alpha_T = -5.0°$; $T_c = 1.300$.

Figure 12.- Continued.

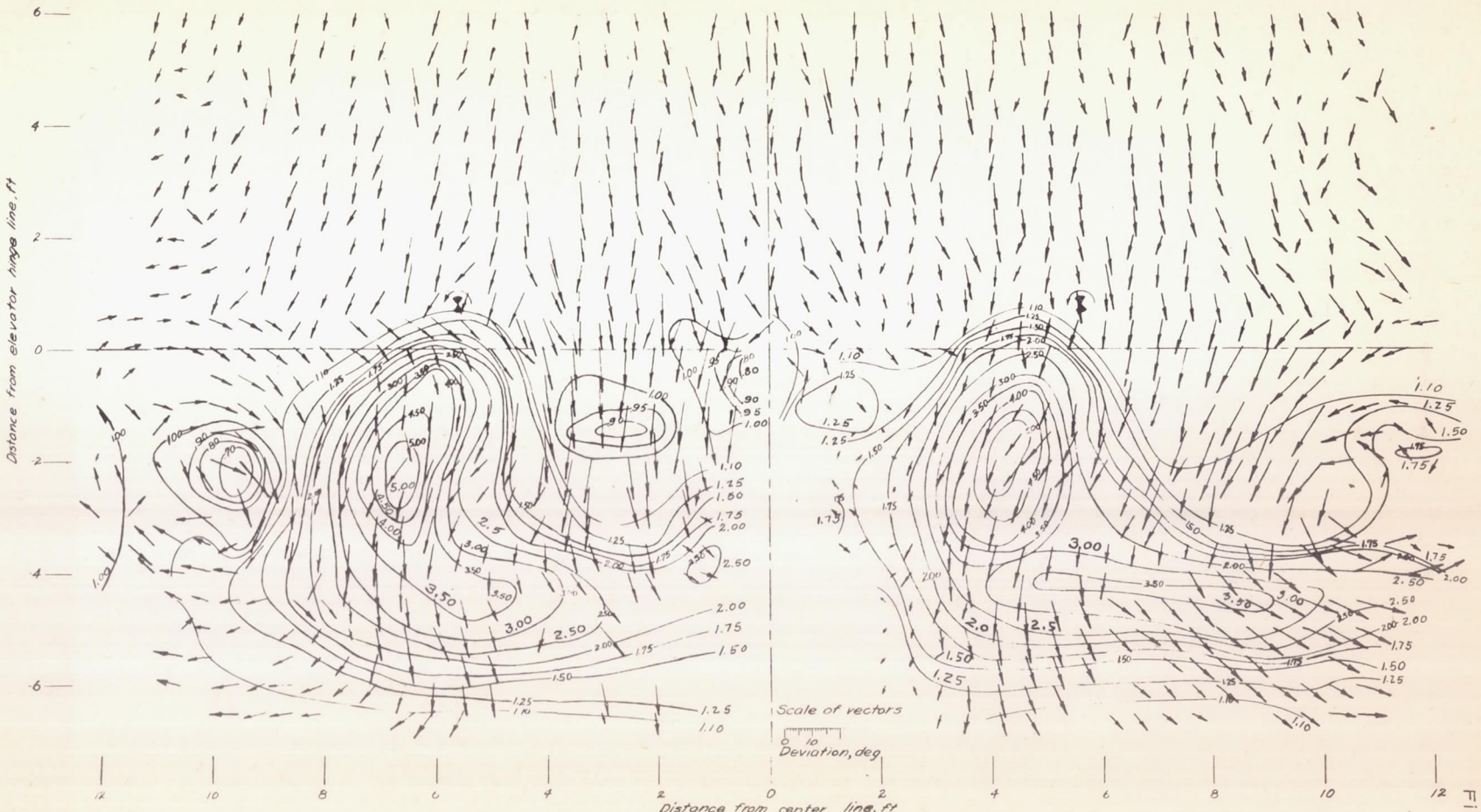

(f) $\alpha_T = 0.3°$; $T_C = 1.300$.

Figure 12.- Continued.

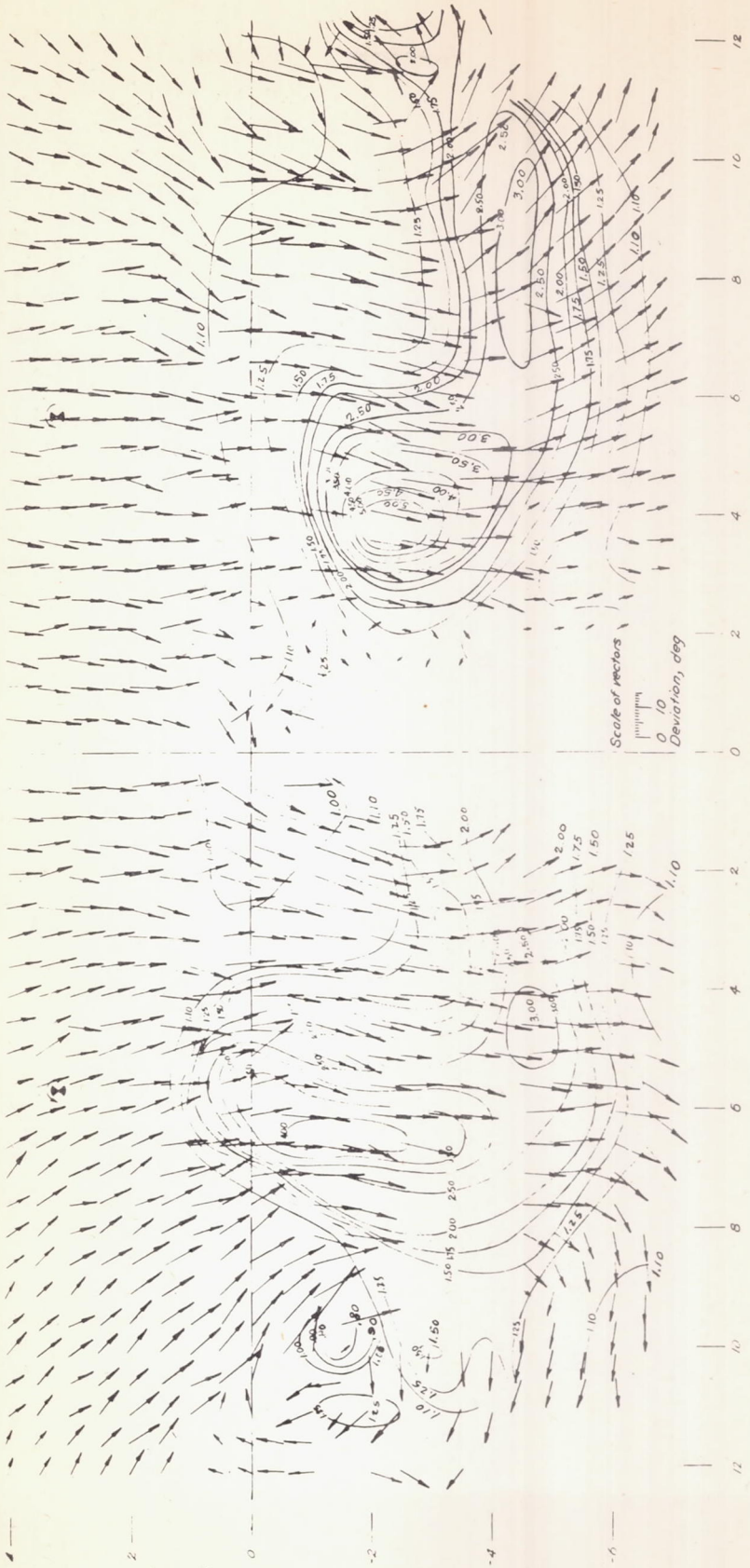

(g) $\alpha_T = 6.8°$; $T_c = 1.300$.

Figure 12 Continued.

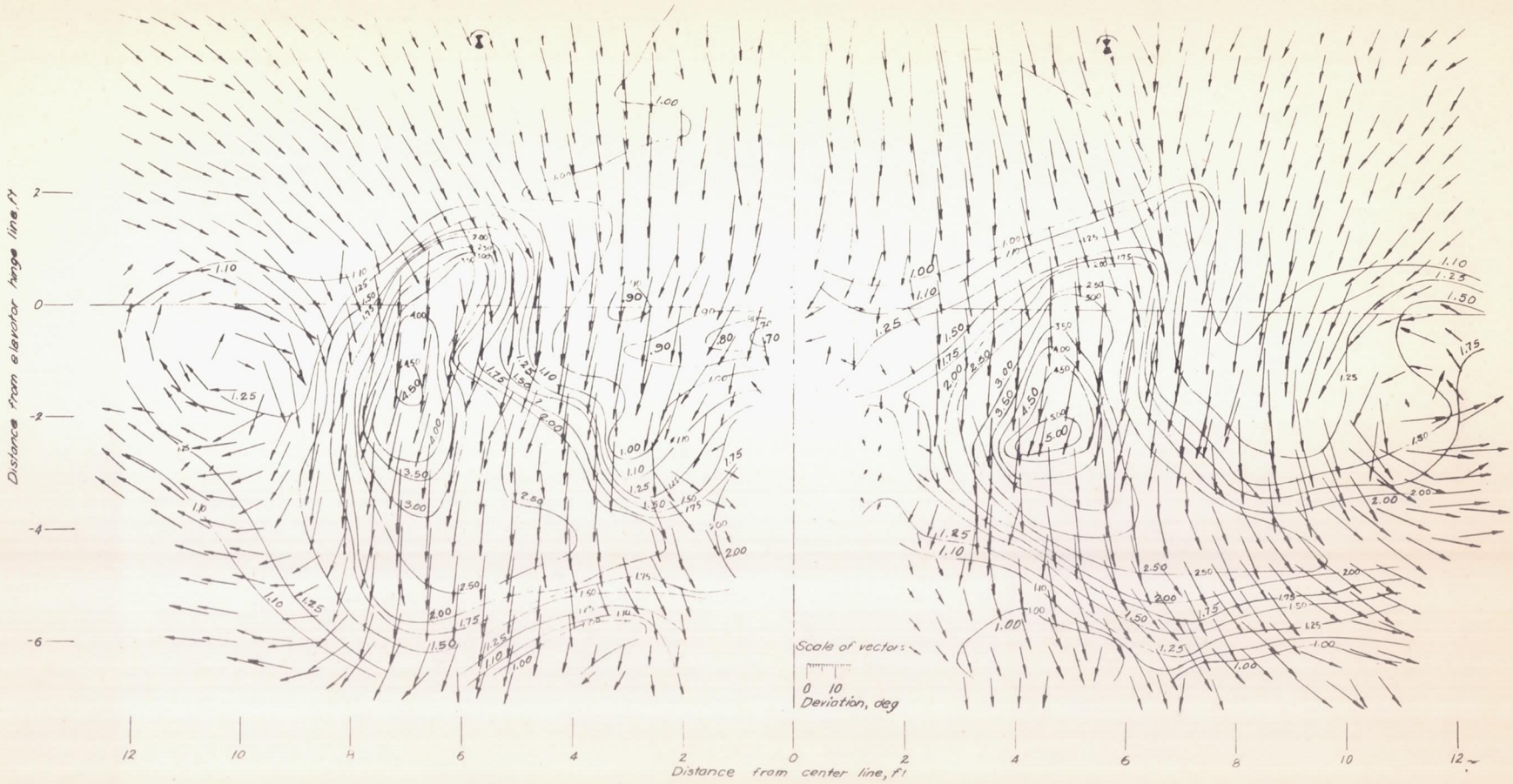

(h) $\alpha_T = 9.6°$, $T_C = 1.300$.

Figure 12.- Concluded.

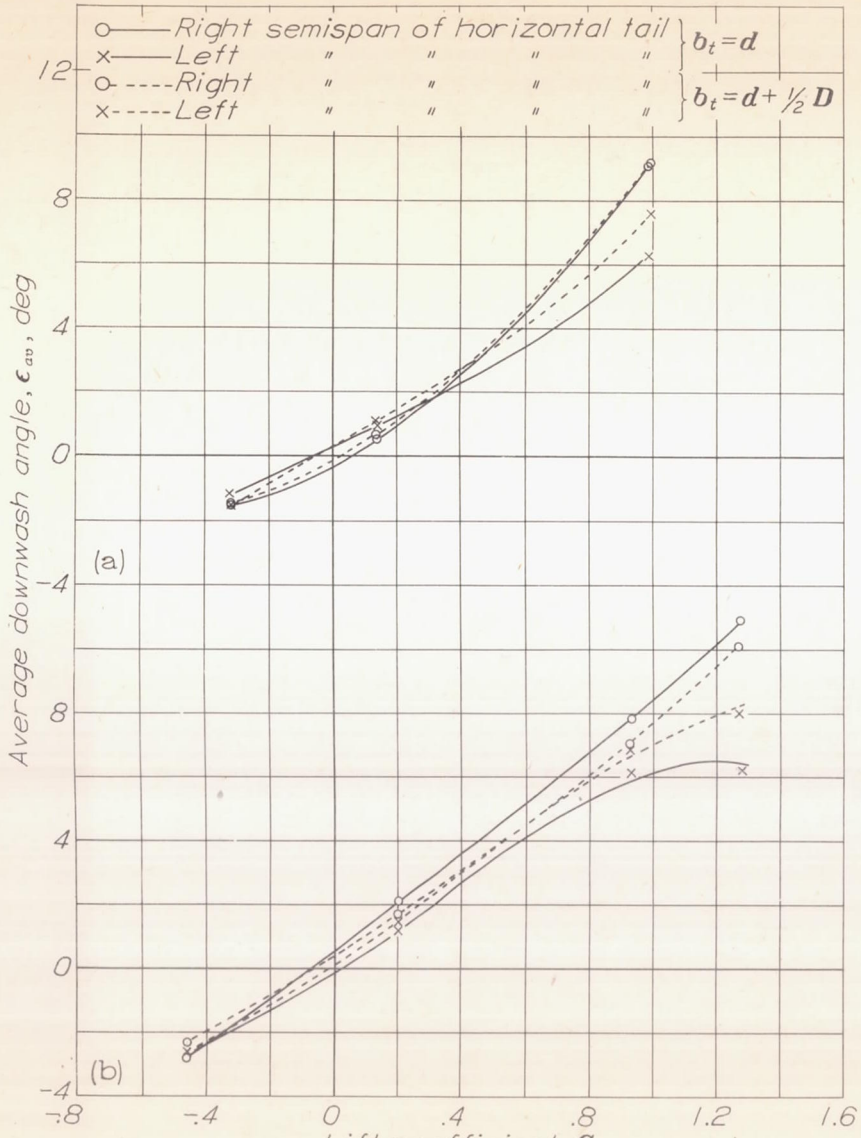

(a) T_c = 0.161. (b) T_c = 1.300.

Figure 16.- Average downwash angles across semispans of horizontal tail surface 12-inches above reference hinge line. Flaps retracted.

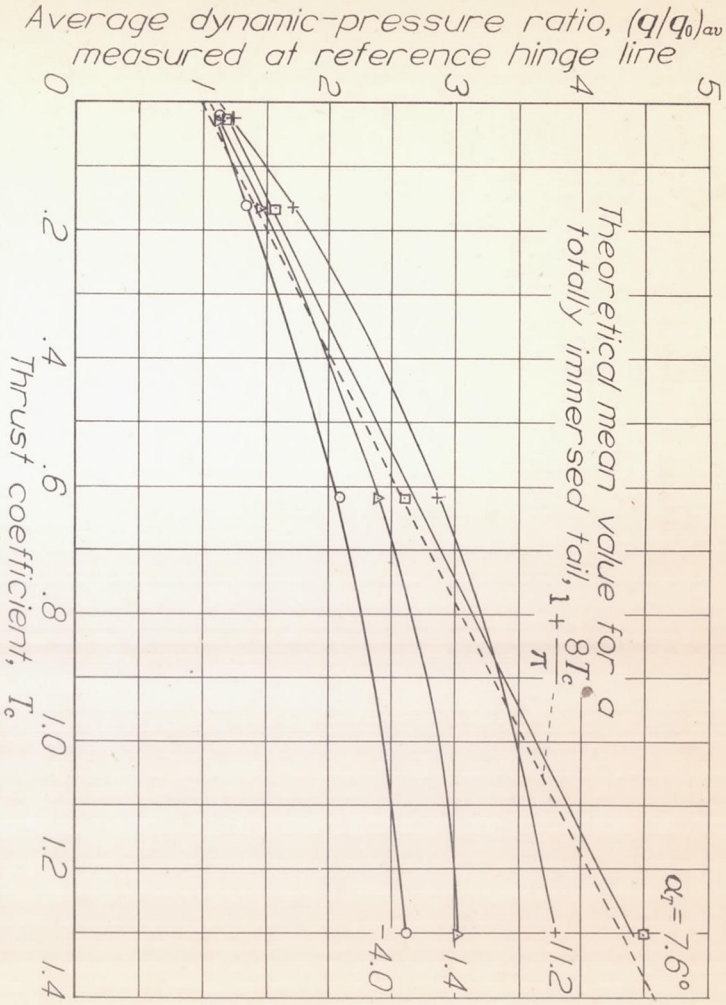

Figure 13.- Comparison between experimental and theoretical $(q/q_0)_{av}$. Flaps retracted; $b_t = d + \frac{1}{2}D$

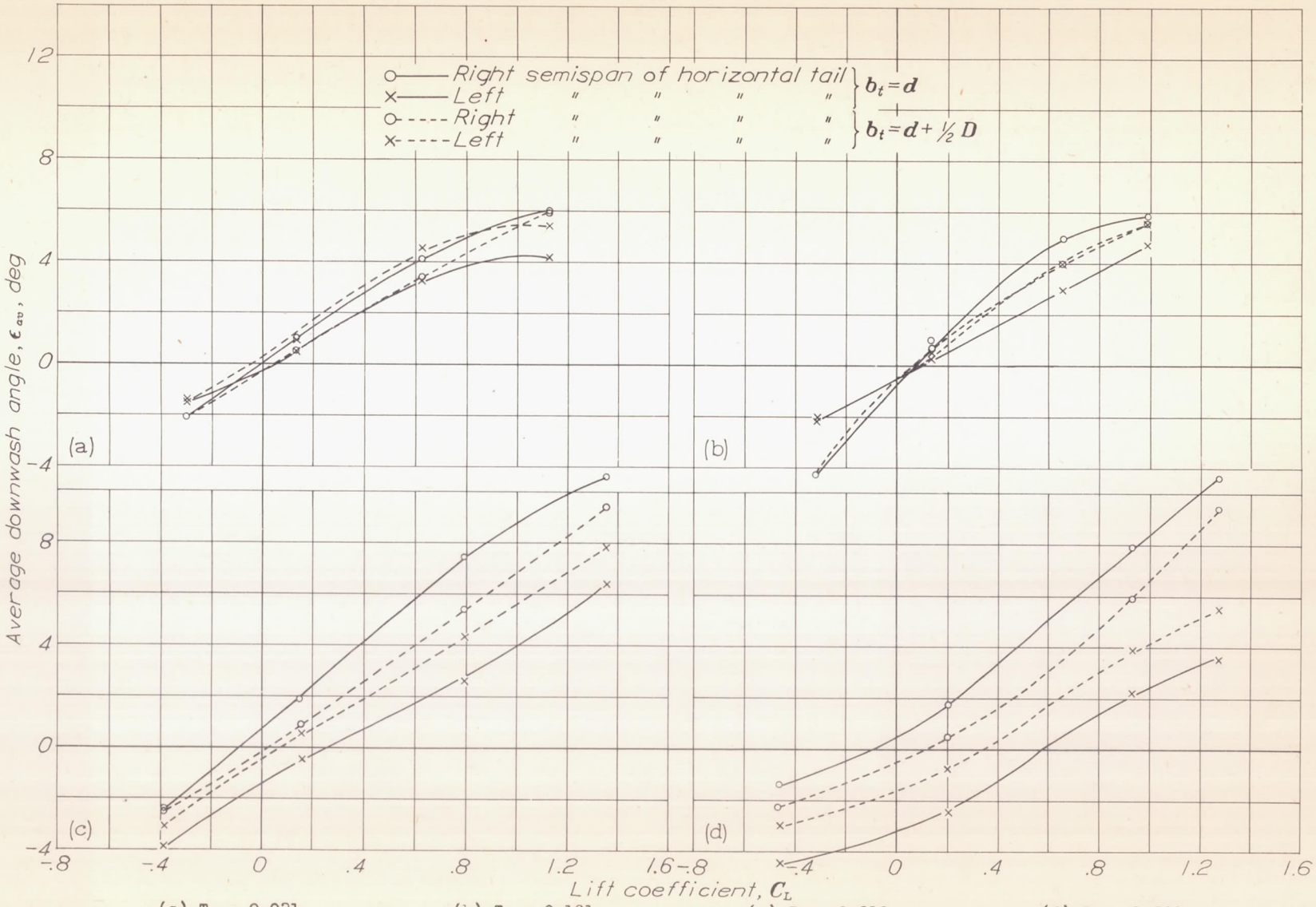

(a) T_c = 0.021. (b) T_c = 0.161. (c) T_c = 0.619. (d) T_c = 1.300.

Figure 14.- Average downwash angles across semispans of horizontal tail surface at reference hinge line. Flaps retracted.

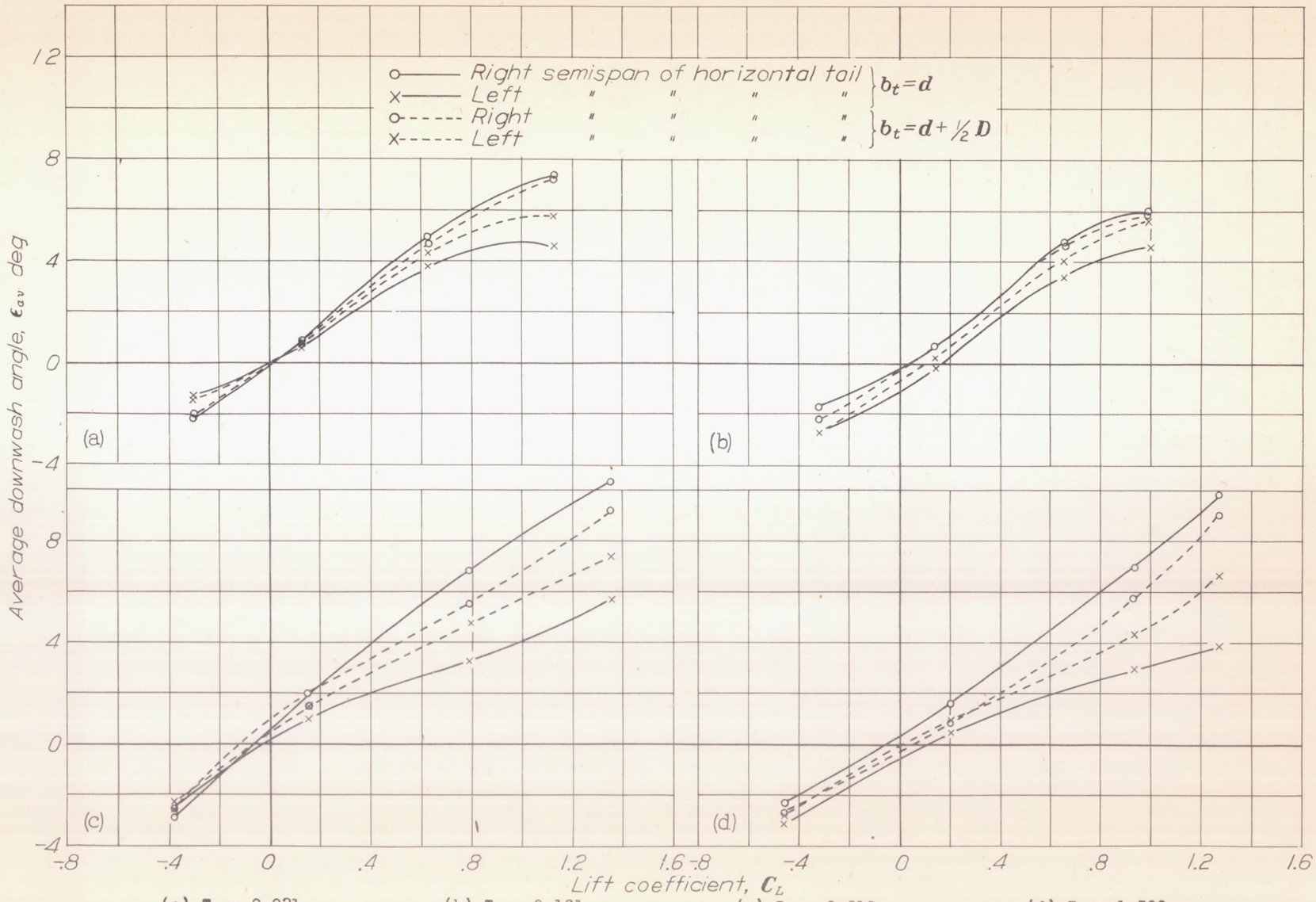

(a) T_c = 0.021. (b) T_c = 0.161. (c) T_c = 0.619. (d) T_c = 1.300.

Figure 15.-Average downwash angles across semispans of horizontal tail surface 6 inches above reference hinge line. Flaps retracted.

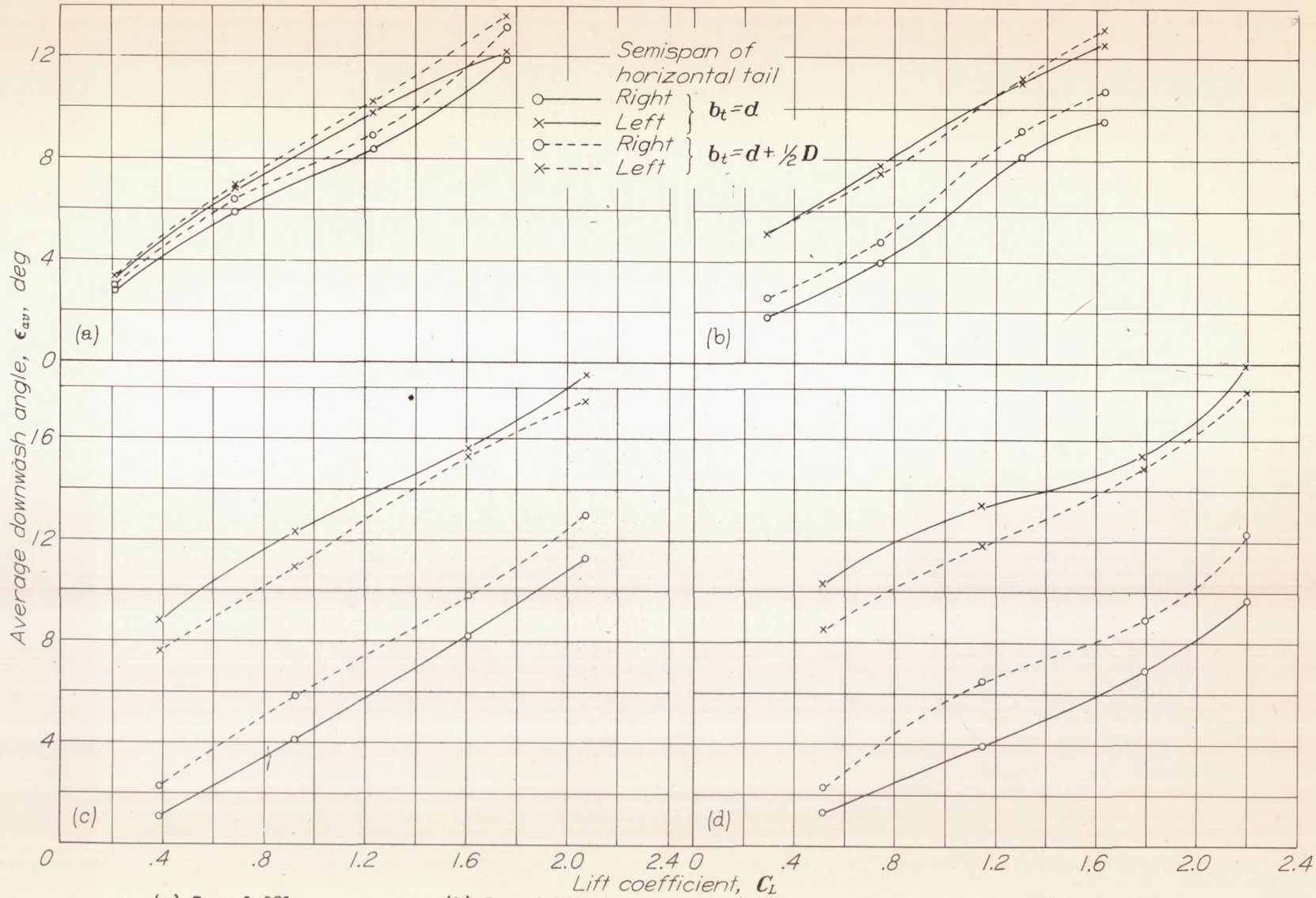

(a) T_c = 0.021. (b) T_c = 0.161. (c) T_c = 0.619. (d) T_c = 1.300.

Figure 17.- Average downwash angles across semispans of horizontal tail surface at reference hinge line. Flaps deflected 50°.

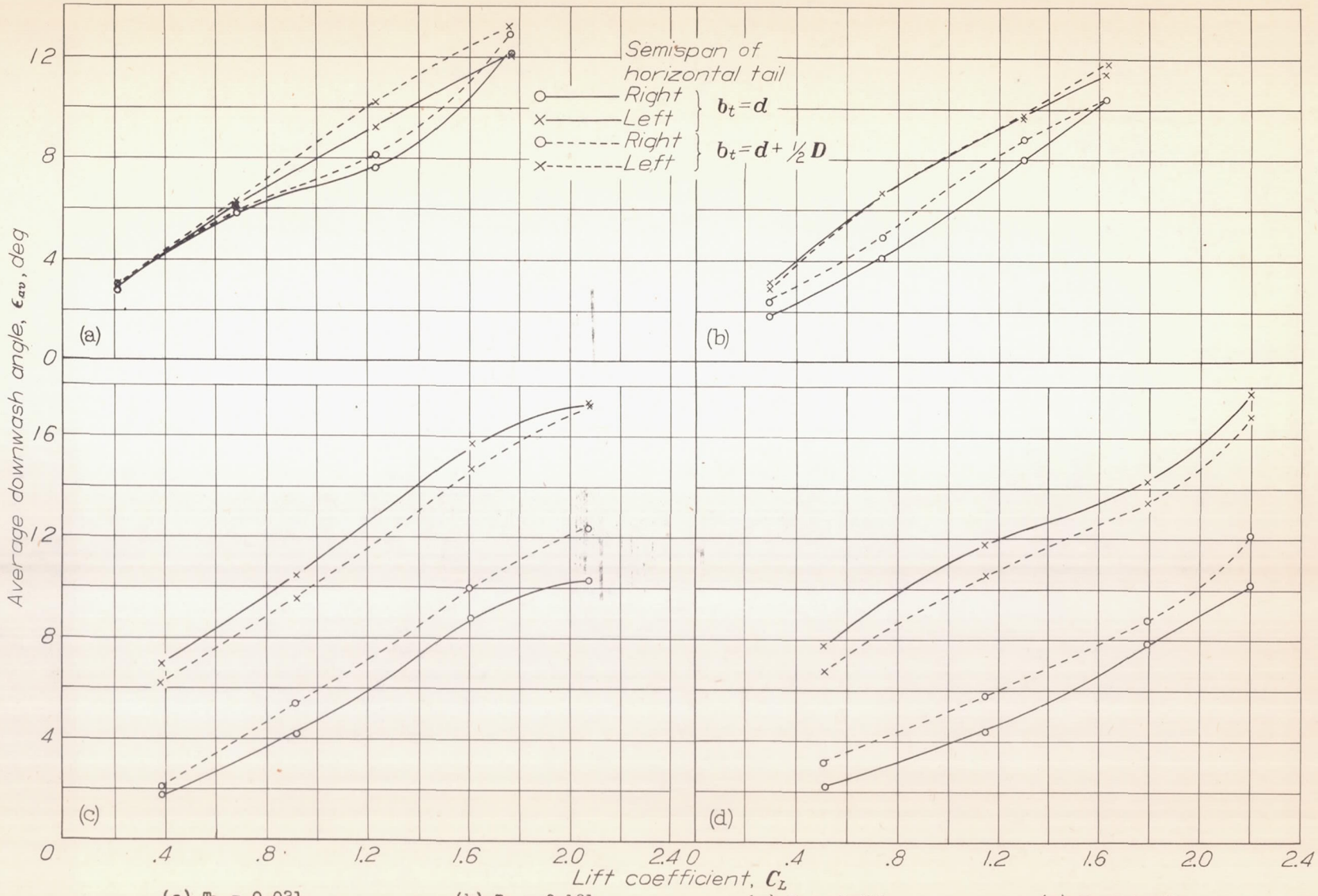

(a) T_c = 0.021. (b) T_c = 0.161. (c) T_c = 0.619. (d) T_c = 1.300.

Figure 18.- Average downwash angles across semispans of horizontal tail surface 6 inches above reference hinge line. Flaps deflected 50°.

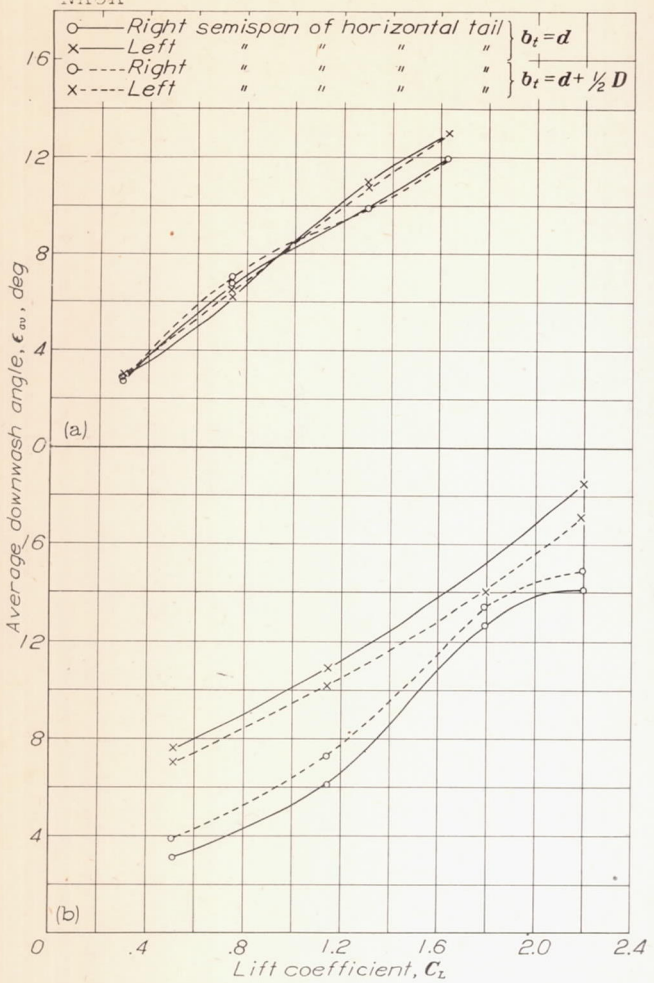

(a) T_c = 0.161. (b) T_c = 1.300.

Figure 19.- Average downwash angles across semispans of horizontal tail surface 12 inches above reference hinge line. Flaps deflected 50°.

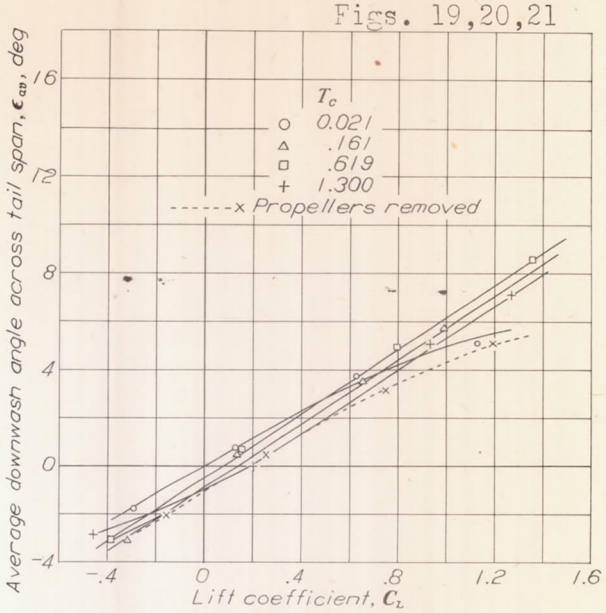

Figure 20.- Variation of ϵ_{av} with C_L for various values of T_c. Measured at reference hinge line; flaps retracted; b_t=d.

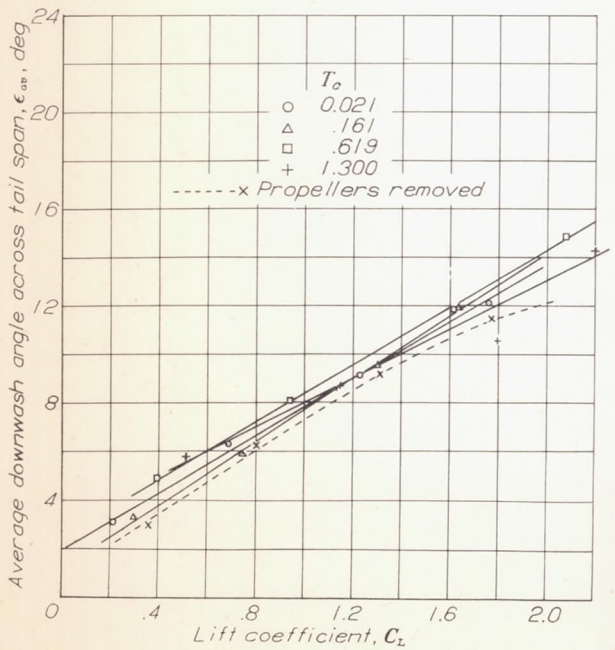

Figure 21.- Variation of ϵ_{av} with C_L for various values of T_c. Measured at reference hinge line; flaps deflected 50°; b_t = d.